CARDIAC HYPERTROPHY

Inhibition of aquaporin-1 prevents myocardial remodeling by blocking the transmembrane transport of hydrogen peroxide

Virginie Montiel[1], Ramona Bella[1], Lauriane Y. M. Michel[1], Hrag Esfahani[1], Delphine De Mulder[1], Emma L. Robinson[2], Jean-Philippe Deglasse[3], Malte Tiburcy[4,5], Pak Hin Chow[6], Jean-Christophe Jonas[3], Patrick Gilon[3], Benjamin Steinhorn[7], Thomas Michel[7], Christophe Beauloye[8], Luc Bertrand[8], Charlotte Farah[1], Flavia Dei Zotti[1], Huguette Debaix[9,10], Caroline Bouzin[11], Davide Brusa[12], Sandrine Horman[8], Jean-Louis Vanoverschelde[8], Olaf Bergmann[13,14], Dimitri Gilis[15], Marianne Rooman[15], Alessandra Ghigo[16], Simonetta Geninatti-Crich[17], Andrea Yool[6], Wolfram H. Zimmermann[4,5,18], H. Llewelyn Roderick[2], Olivier Devuyst[9,10], Jean-Luc Balligand[1]*

Pathological remodeling of the myocardium has long been known to involve oxidant signaling, but strategies using systemic antioxidants have generally failed to prevent it. We sought to identify key regulators of oxidant-mediated cardiac hypertrophy amenable to targeted pharmacological therapy. Specific isoforms of the aquaporin water channels have been implicated in oxidant sensing, but their role in heart muscle is unknown. RNA sequencing from human cardiac myocytes revealed that the archetypal *AQP1* is a major isoform. *AQP1* expression correlates with the severity of hypertrophic remodeling in patients with aortic stenosis. The AQP1 channel was detected at the plasma membrane of human and mouse cardiac myocytes from hypertrophic hearts, where it colocalized with NADPH oxidase-2 and caveolin-3. We show that hydrogen peroxide (H_2O_2), produced extracellularly, is necessary for the hypertrophic response of isolated cardiac myocytes and that AQP1 facilitates the transmembrane transport of H_2O_2 through its water pore, resulting in activation of oxidant-sensitive kinases in cardiac myocytes. Structural analysis of the amino acid residues lining the water pore of AQP1 supports its permeation by H_2O_2. Deletion of *Aqp1* or selective blockade of the AQP1 intrasubunit pore inhibited H_2O_2 transport in mouse and human cells and rescued the myocyte hypertrophy in human induced pluripotent stem cell–derived engineered heart muscle. Treatment of mice with a clinically approved AQP1 inhibitor, Bacopaside, attenuated cardiac hypertrophy. We conclude that cardiac hypertrophy is mediated by the transmembrane transport of H_2O_2 by the water channel AQP1 and that inhibitors of AQP1 represent new possibilities for treating hypertrophic cardiomyopathies.

INTRODUCTION

Myocardial remodeling is a prequel to heart failure. It involves profound structural and functional alterations in cardiac tissue driven by hemodynamic stress, inflammation, and neurohumoral stimulation. Hypertrophy of cardiac myocytes largely contributes to alterations in ventricular compliance that, combined with gene expression reprogramming and loss of contractility, leads to loss of diastolic and systolic functions (*1*, *2*). Oxidative stress is a common pathogenic feature underlying these phenomena, but the actual identity, sources, and distribution of the reactive oxygen species (ROS) involved in different myocardial cell types remain unclear. This may explain the failure of previous clinical trials in which antioxidants have been applied systemically (*3*, *4*), pointing to the need for a more detailed understanding of ROS signaling and regulation in the myocardium.

There are many potential sources of ROS in the stressed myocardium, either from paracrine sources (e.g., from inflammatory cells) or from within cardiac myocytes themselves. Mitochondria, xanthine oxidoreductase, reduced form of nicotinamide adenine dinucleotide phosphate (NADPH) oxidases, and uncoupled nitric oxide synthases (NOSs) all are recognized producers of ROS in different compartments

[1]Institute of Experimental and Clinical Research (IREC), Pharmacology and Therapeutics (FATH), Cliniques Universitaires St Luc and Université Catholique de Louvain (UCLouvain), 1200 Brussels, Belgium. [2]Laboratory of Experimental Cardiology, Department of Cardiovascular Sciences, KULeuven, 3000 Leuven, Belgium. [3]Institute of Experimental and Clinical Research (IREC), Endocrinology, Diabetes and Nutrition (EDIN), Université Catholique de Louvain (UCLouvain), 1200 Brussels, Belgium. [4]Institute of Pharmacology and Toxicology, University Medical Center Göttingen, 37075 Göttingen, Germany. [5]DZHK (German Center for Cardiovascular Research), Partner Site Göttingen, 37075 Göttingen, Germany. [6]Adelaide Medical School, University of Adelaide, Adelaide, SA 5000, Australia. [7]Cardiovascular Division, Department of Medicine, Brigham and Women's Hospital, Harvard Medical School, Boston, MA 2115, USA. [8]Institute of Experimental and Clinical Research (IREC), Pole of Cardiovascular Research (CARD), Cliniques Universitaires St Luc and Université Catholique de Louvain (UCLouvain), 1200 Brussels, Belgium. [9]Institute of Experimental and Clinical Research (IREC), Nephrology (NEFR), Cliniques Universitaires St Luc and Université Catholique de Louvain (UCLouvain), 1200 Brussels, Belgium. [10]Institute of Physiology, University of Zürich, CH 8057 Zürich, Switzerland. [11]2IP-IREC Imaging Platform, Institute of Experimental and Clinical Research (IREC), Université Catholique de Louvain (UCLouvain), 1200 Brussels, Belgium. [12]Flow Cytometry Platform, Institute of Experimental and Clinical Research (IREC), Université Catholique de Louvain (UCLouvain), 1200 Brussels, Belgium. [13]Center for Regenerative Therapies Dresden, Technische Universität Dresden, 01062 Dresden, Germany. [14]Department of Cell and Molecular Biology, Karolinska Institutet, 171 77 Stockholm, Sweden. [15]Computational Biology and Bioinformatics (3BIO-BioInfo), Université Libre de Bruxelles (ULB), 1000 Brussels, Belgium. [16]Molecular Biotechnology Center, Università di Torino, 10124 Torino, Italy. [17]Molecular Biotechnology and Health Sciences, Università di Torino, 10124 Torino, Italy. [18]Cluster of Excellence "Multiscale Bioimaging: from Molecular Machines to Networks of Excitable Cells" (MBExC), University of Göttingen, 37075 Göttingen, Germany.
*Corresponding author. Email: jl.balligand@uclouvain.be

of cardiac myocytes. Recent advances have highlighted the pathogenic role of ROS and nitrosating species in the development of heart failure (*5*, *6*), specifically of hydrogen peroxide (H_2O_2) in cardiac myocytes (*7*, *8*). The identification of key regulators of its distribution, particularly in specific subcellular compartments, is paramount for the design of targeted therapies.

Aquaporins (AQPs) are a family of water channels with large tissue/cell distribution (*9*). Several isoforms are expressed in cardiac and vascular tissues, e.g., AQP1, AQP4, AQP7, and AQP8 in the mouse heart (*10*). Some AQP isoforms may transport other molecules in addition to water, e.g., glycerol for the "aquaglyceroporins" (AQP3, AQP7, AQP9, and AQP10) or ammonia and/or H_2O_2 for the "peroxiporins" (*11*). The latter include AQP3 (*12*), AQP8 (*13*), and AQP9 (*14*), which were shown to mediate H_2O_2 import and/or signaling in inflammatory or cancer cell lines in vitro. Whether these or other AQP isoforms mediate oxidant signaling in specific cardiac cell types is unknown. No cardiac phenotype has been described so far in mice after knockout of *Aqp8* (*15*), *Aqp3*, or *Aqp9* (*16*). Conversely, genetic deficiency in *Aqp1* results in microcardia, with smaller cardiac myocytes compared with wild-type littermates (*10*, *17*). *AQP1* transcripts were also found to be expressed in the stressed human myocardium, including failing hearts (*18*, *19*), without clear identification of the cell type of origin. Moreover, the role of AQP1 in the modulation of cardiac myocyte hypertrophy is unknown, let alone its involvement in H_2O_2 transport in the heart.

RESULTS

AQP1 expression in mouse and human cardiac myocytes and relationship to myocardial hypertrophy

The mouse heart expresses transcripts for *Aqp1*, *Aqp4*, *Aqp7*, and *Aqp8*, as detected by reverse transcription quantitative polymerase chain reaction (RT-qPCR), as well as the corresponding proteins by immunoblotting (*10*). However, only AQP1, AQP4, and AQP7 proteins are found in plasma membrane fractions, whereas AQP8 is detected exclusively in cytosolic membrane fractions (*10*), including the endoplasmic reticulum (*19*). We first confirmed the expression of AQP1 and AQP4 proteins in isolated adult mouse cardiac myocytes (Fig. 1A and fig. S1A). We next analyzed *AQP* transcripts differentially expressed in human cardiac myocytes from healthy and hypertrophic hearts (Fig. 1B). Human hypertrophic myocardium expressed genes typically associated with remodeling (*NPPA*, *NPPB*, *MYH7*, and *TNNT2*), as expected (fig. S1B). To restrict our analysis to cardiac myocytes, cell-specific RNA was isolated from flow-sorted pericentriolar material 1–positive cardiac myocyte nuclei, and the transcriptome was profiled by RNA sequencing (RNA-seq). This approach allows isolation of RNA highly enriched in marker genes and processes that are specific to cardiac myocytes (*20*). Among all *AQP* isoforms, we found *AQP1* to be actively transcribed in healthy and hypertrophic myocytes (Fig. 1B and fig. S1, C and D). Further analysis restricted to mature RNA by RT-qPCR from the same nuclei revealed *AQP1* to be up-regulated in hypertrophic myocytes

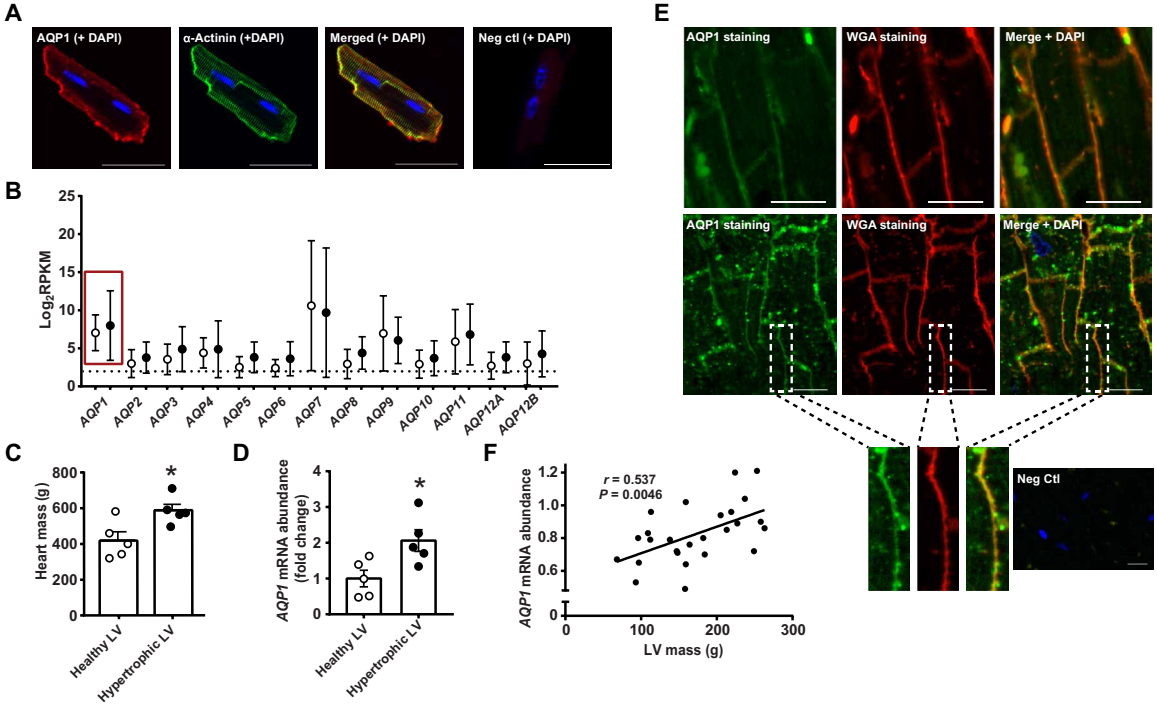

Fig. 1. Expression of AQP1 in human and mouse cardiac myocytes and relationship to hypertrophy. (**A**) Representative image of AQP1 immunostaining in adult mouse cardiac myocytes [red staining, AQP1; green staining, α-sr-actinin; blue staining, 4′,6-diamidino-2-phenylindole (DAPI)]. Neg Ctl, absent immunostaining after omission of primary anti-AQP1 antibody in presence of the secondary anti–immunoglobulin G antibody. Scale bar, 50 μM. (**B**) Quantification of *AQP* expression as reads per kilobase per million reads (RPKM) from RNA-seq data of transcripts from pericentriolar material 1–positive ($PCM1^+$) nuclei (cardiac myocytes) isolated from healthy control (open circles) and left ventricle (LV) hypertrophic myocardium (closed circles; means ± SEM; $N = 4$ independent experiments, each running a healthy and a hypertrophic sample in parallel). Intronic and exonic reads were counted. (**C**) Human total heart mass as measured postmortem (table S1; $N = 5$ patients each). (**D**) *AQP1* mature mRNA expression in healthy versus LV hypertrophic $PCM1^+$ nuclei as measured by RT-qPCR and normalized to the geometric mean of *GAPDH*, *ACTB*, and *B2M*. Each dot is representative of triplicate measurements by RT-qPCR; $N = 5$ patients each, from (C). *$P < 0.05$ by Student's *t* test. (**E**) Representative histological section of human LV healthy (top) and hypertrophic (bottom) myocardium from a patient with aortic stenosis [green staining, AQP1; red staining, wheat germ agglutinin (WGA); blue staining, DAPI]. Scale bars, 10 μM. Neg Ctl, immunostaining without primary AQP1 antibody in presence of secondary antibody. (**F**) Correlation between abundance of human *AQP1* transcripts in biopsy samples of LV myocardium and LV mass, measured preoperatively by echocardiography. Each dot is representative of triplicate measurements by RT-qPCR (normalized to *GAPDH*). $N = 26$ patients.

(Fig. 1, C and D), whereas other highly expressed *AQP* isoforms (*AQP4*, *AQP7*, and *AQP9*) were unchanged (fig. S1, E to G). Gene ontology pathway analysis revealed an enrichment of biological processes related to oxidative stress in cardiac myocytes from hypertrophic myocardium (fig. S1H). We confirmed AQP1 protein expression at the peripheral membrane of human cardiac myocytes in biopsy specimens from patients with or without cardiac hypertrophy (Fig. 1E). Moreover, RT-qPCR analysis of mRNA isolated from biopsy samples from patients with aortic stenosis revealed a positive correlation between *AQP1* mRNA expression and degree of hypertrophy (as measured by preoperative echocardiography) (Fig. 1F), further suggesting relevance to human pathology.

Attenuated hypertrophy in AQP1-deficent mice

We next used *Aqp1*-deficient mice to test the function of AQP1 in the development of hypertrophy in vivo. Knockout ($Aqp1^{-/-}$), heterozygous ($Aqp1^{+/-}$; with 50% reduction of AQP1 protein; fig. S2A), and wild-type ($Aqp1^{+/+}$) littermates were either subjected to transverse aortic constriction (TAC; Fig. 2, A to I) or minipump infusion of angiotensin II (Ang II; Fig. 2, J to L). The dose of Ang II (2.0 mg/kg per day for 2 weeks) was selected on the basis of preliminary experiments, showing similar hypertrophy at this dose compared with 1.2 or 2.0 mg/kg per day for 4 weeks in this SV129 mouse background. Both TAC and Ang II infusion induced the expected hypertrophic remodeling, including myocyte hypertrophy and interstitial fibrosis in $Aqp1^{+/+}$ mice. However, these effects were attenuated in $Aqp1^{-/-}$ mice, despite similar trans-stenotic gradients after TAC (verified by echocardiography; fig. S2B) or similar increases in peripheral blood pressure after Ang II (verified by implanted telemetry in awake mice; fig. S2C). The attenuated cardiac hypertrophy was associated with lower expression of genes characteristic of hypertrophic remodeling, e.g., *Nppb* and *Myh7* (Fig. 2, G and H), as well as decreased immunolabeled collagen type I, alpha-1 (COL1A1) protein (Fig. 2F), whole collagen content, and packing/alignment reflected by color hue under polarized light (Fig. 2E). The heterozygous $Aqp1^{+/-}$ mice developed an intermediate phenotype (Fig. 2A), confirmed by histomorphometric measurements (Fig. 2, B to D). Although *Aqp1*-deficient mice exhibited milder concentric hypertrophy (Tables 1 and 2), they did not develop clinical or echocardiographic signs of heart failure up to 9 weeks after TAC (Table 1).

Rescue of cardiac myocyte hypertrophy by deletion or pharmacologic blockade of AQP1

To verify that AQP1 modulates hypertrophy in the cardiac myocytes themselves, rather than through indirect paracrine effects, we used primary cultured cells isolated from the *Aqp1*-deficient mice and tested their response to a variety of prohypertrophic stimuli (Fig. 3, A to E). Cardiac myocytes from $Aqp1^{+/+}$ mice developed hypertrophy in response to Ang II (Fig. 3B), endothelin-1 (Fig. 3C), isoproterenol (nonspecific β-adrenergic agonist; Fig. 3D), and phenylephrine (α_1-adrenergic agonist; Fig. 3E), paralleled with increased incorporation of ^{14}C-phenyl-alanine reflecting increased protein synthesis (fig. S2D). These hypertrophic effects were abrogated in myocytes from $Aqp1^{-/-}$ mice (Fig. 3, A to E, and fig. S2D), demonstrating that specific expression of AQP1 in the cardiac myocyte is necessary for the development of hypertrophy in response to neurohumoral agonists.

Because genetic deletion of *Aqp1* may induce changes in other effectors within shared macromolecular complexes that regulate signaling, we repeated these experiments with pharmacologic blockers of AQP1. AQP1 channels are organized in tetramers in the plasma membrane, with water transport being mediated through the individual intrasubunit pore of each monomer, whereas monovalent ions (Na^+ and K^+) may permeate through the central channel formed by the four monomers (*21*). We therefore used specific blockers of each form of transport, namely, Bacopaside II and AqB011, respectively (Fig. 3F). AqB011, a blocker of the ionic central channel (*22*), did not influence the hypertrophy of $Aqp1^{+/+}$ cardiac myocytes treated with phenylephrine. Conversely, Bacopaside II, a specific blocker of the intrasubunit water pore (*23*), fully blocked the hypertrophic response in these cells. Together, these data clearly showed that AQP1 contributes to the hypertrophic response of cardiac myocytes through permeability of its water channel.

We next evaluated the impact of *Aqp1* deletion on rapid water transport across the membrane of isolated adult mouse cardiac myocytes. Changes in volume of fluorescently labeled myocytes were used as a surrogate of water-induced swelling and validated by comparison with water proton low-field nuclear magnetic resonance (^{1}H-NMR) relaxometry (Fig. 3, G and H, and fig. S3). Incubation of myocytes in hypo-osmotic (100 mOsm/liter) buffer induced swelling (Fig. 3G), as well as increased water residence time (Fig. 3H), indicative of rapid water influx in $Aqp1^{+/+}$ cardiac myocytes; hypo-osmotic water transit was identical in myocytes from $Aqp1^{-/-}$ mice, probably due to compensatory transport by other AQP (e.g., AQP4). Short-term stimulation with phenylephrine in iso-osmotic solution produced minimal swelling of cardiac myocytes (Fig. 3I), which, similar to hypo-osmotic stress, was not different between genotypes. Therefore, AQP1 is dispensable for the rapid water movements across the membrane of cardiac myocytes, whereas it is necessary for hypertrophy.

Extracellular hydrogen peroxide from NADPH oxidase as mediator of cardiac myocyte hypertrophy

ROS from different sources differentially mediate hypertrophic signaling and/or contractile dysfunction in cardiac myocytes (*24*). By proximity ligation assays, we observed a colocalization of the $p47^{phox}$ subunit of NADPH oxidase-2 (NOX2) with the caveolar coat protein caveolin-3 at the peripheral plasma membrane (Fig. 4A), confirming its confinement to caveolin-enriched membrane fractions (*25*). $p47^{phox}$ also colocalized with AQP1 at the peripheral membrane (Fig. 4B). The colocalization signal was increased upon myocyte stimulation with Ang II (Fig. 4B, bottom), whereas it was absent in negative control experiments. The association of $p47^{phox}$ with caveolin-3 after Ang II superfusion was preserved in cardiac myocytes from $Aqp1^{-/-}$ mice (Fig. 4A), showing that the deletion of AQP1 does not interfere with the assembly of NOX2 subunits necessary for its activation at the membrane. These results suggested a colocalization of AQP1 and NOX2 in the caveolin-3–enriched peripheral membrane, with an increased assembly of functional NOX upon treatment with Ang II.

We next tested the involvement of NOX2 as a source of prohypertrophic ROS. In adult mouse cardiac myocytes, coincubation with the pan-NOX inhibitor VAS2870 (*26*) at a concentration known to preferentially inhibit NOX2 (*27*) abrogated the hypertrophic response to all four neurohumoral agonists (Fig. 4C), pointing to NOX as a main source of ROS for promoting hypertrophy.

Plasmalemma-associated NOX are known to produce superoxide anions in the extracellular space (*28*), where they are rapidly dismutated to H_2O_2 by the extracellular superoxide dismutase (or SOD3) (*29*). To confirm the involvement of extracellular H_2O_2 in

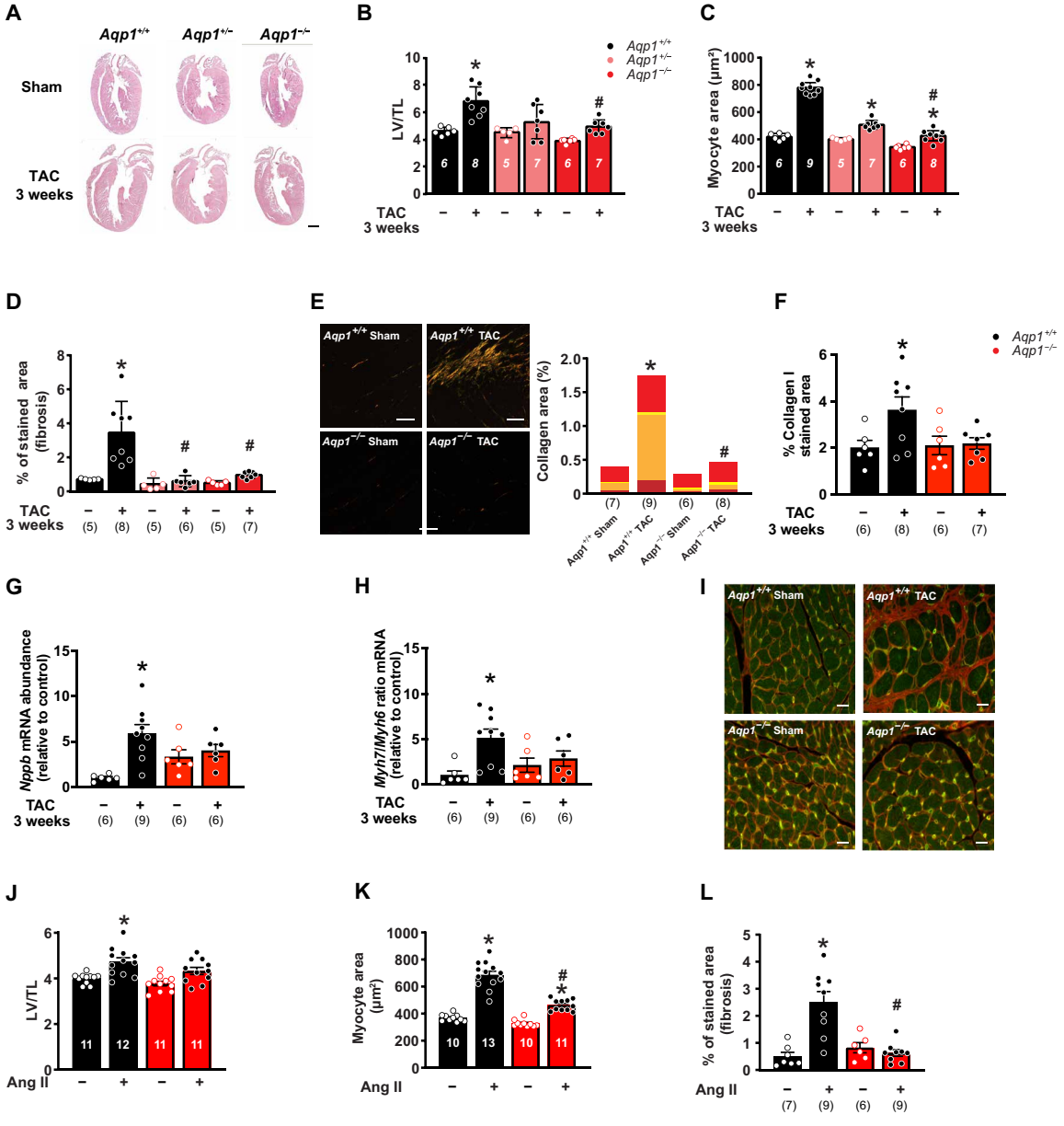

Fig. 2. AQP1 deletion attenuates myocardial hypertrophy and fibrosis. (**A** to **I**) Morphometric and histologic assessment of remodeling in $Aqp1^{+/+}$, $Aqp1^{+/-}$, and $Aqp1^{-/-}$ mice subjected to TAC or sham for 3 weeks. (*N* mice indicated in bars or below the *x* axis). (A) Hematoxylin and eosin staining of longitudinal sections of hearts from mice of different genotypes after TAC or sham operation. Scale bar, 1 mm. (B) LV mass normalized to tibial length (TL). (C) Myocyte transverse area measured histologically (WGA staining; each dot is mean from >200 myocytes per heart). (D) Interstitial fibrosis (Picrosirius red staining; % section area; each dot is mean from three sections per heart). (E) Quantification of collagen content using polarized light microscopy on Picrosirius red–stained heart sections from $Aqp1^{+/+}$ and $Aqp1^{-/-}$ mice subjected to TAC or sham operation. Representative images and quantification of the total collagen content and proportion of collagen fibers are defined by color hue, representing the relative increase in collagen thickness and packing/alignment from yellow to red. (F) Quantification of COL1A1 protein by immunostaining (each dot is mean from three sections per heart). (G and H) Hypertrophic transcriptional program assessed by (G) *Nppb* mRNA abundance (RT-qPCR) or (H) relative *Myh7*/*Myh6* mRNA abundance (RT-qPCR). (I) Representative histological section of LV myocardium of $Aqp1^{+/+}$ and $Aqp1^{-/-}$ mice 3 weeks after TAC or sham (green staining, isolectin; red staining, WGA). Scale bars, 20 μM. (**J** to **L**) Morphometric and histologic assessment of remodeling in $Aqp1^{+/+}$ and $Aqp1^{-/-}$ mice subjected to minipump infusion of angiotensin II (Ang II; 2 mg/kg per day) or physiological solution for 14 days (*N* mice indicated in bars or below the *x* axis). (J) LV mass normalized to tibial length. (K) Myocyte transverse area measured histologically (WGA staining; each dot is mean from >200 myocytes per heart). (L) Interstitial fibrosis (Picrosirius red staining; % section area; each dot is mean from three sections per heart). Means ± SEM; **P* < 0.05 versus solvent Ctl; #*P* < 0.05 versus Ang II or TAC by two-way ANOVA, followed by Tukey's correction for multiple comparisons, except (H) **P* < 0.05 by Kruskal-Wallis, corrected for multiple comparisons with Dunn's test, and (F and J) **P* < 0.05 by one-way ANOVA, corrected for multiple comparisons with Sidak's test.

the hypertrophic response, adult cardiac myocytes from $Aqp1^{+/+}$ mice were stimulated with phenylephrine with or without incubation with non–polyethylene glycol (PEG)–ylated (i.e., membrane-impermeable) catalase, followed by measurement of hypertrophy (Fig. 5A). Catalase had no effect on myocyte size when applied alone, but it fully abrogated induction of hypertrophy by phenylephrine when coincubated with the latter (Fig. 5A). As expected, no hypertrophy or effect of catalase was observed in $Aqp1^{-/-}$ myocytes. Similar effects were observed in neonatal mouse cardiac myocytes (Fig. 5B).

ROS activate specific oxidant-sensitive kinases that relay the prohypertrophic signal in cardiac myocytes. Accordingly, we observed an increase in immunoblotted phospo-p38 and phospho–extracellular signal–regulated kinase (ERK) mitogen-activated protein kinases (MAPKs) in response to phenylephrine in adult cardiac myocytes from $Aqp1^{+/+}$ mice (Fig. 5, C to G). This increase in ERK

Table 1. Echocardiographic parameters in *Aqp1*$^{+/+}$ and *Aqp1*$^{-/-}$ mice submitted to TAC for 3 or 9 weeks. Results are means ± SEM. Mixed-effect model with repeated measures (Tukey post hoc test for TAC effect; Sidak post hoc test for genotype effect). TAC, transverse aortic constriction; HR, heart rate; LVEDv, left ventricle end-diastolic volume; LVESv, left ventricle end-systolic volume; EF, ejection fraction; IVSd, interventricular septum thickness in diastoly; LVIDd, left ventricle internal diameter in diastoly; PWd, posterior wall thickness in diastoly; FS, fractional shortening; RWT, relative wall thickness; LVmass, left ventricular mass; Ao vel, (transgradient) aortic velocity; KO, knockout; bpm, beats per minute.

	WT			AQP1 KO		
	Pre-op (n = 16)	TAC 3 weeks (n = 7)	TAC 9 weeks (n = 9)	Pre-op (n = 16)	TAC 3 weeks (n = 7)	TAC 9 weeks (n = 9)
HR (bpm)	401 ± 8	379 ± 14	363 ± 17*	365 ± 11**	340 ± 15	377 ± 12
LVEDv (μl)	74.8 ± 2.2	70.5 ± 3.9	67.7 ± 2.8	60.3 ± 3.0**	64.9 ± 4.1	58.0 ± 1.8
LVESv (μl)	40.7 ± 2.6	40.5 ± 4.6	35.6 ± 1.4	31.0 ± 2.6**	34.8 ± 2.6	31.6 ± 2.2
EF (%) B mode	46.2 ± 2.2	43.1 ± 4.0	47.2 ± 1.7	49.5 ± 2.6	46.2 ± 2.6	45 ± 2.9
IVSd (mm)	0.83 ± 0.03	0.97 ± 0.04*	0.97 ± 0.05*	0.68 ± 0.01**	0.82 ± 0.07*	0.82 ± 0.04*,***
LVIDd (mm)	4.20 ± 0.04	4.14 ± 0.08	4.14 ± 0.08	4.02 ± 0.13	3.94 ± 0.13	3.94 ± 0.09
PWd (mm)	0.78 ± 0.03	1.03 ± 0.05*	0.91 ± 0.02*	0.68 ± 0.02	0.90 ± 0.10	0.82 ± 0.05*
FS (%) M-mode	21.5 ± 1.1	21.5 ± 2.6	22.0 ± 1.0	23.7 ± 1.5	23.8 ± 2.2	21.0 ± 1.5
RWT	0.39 ± 0.01	0.48 ± 0.02*	0.46 ± 0.01*	0.34 ± 0.01	0.44 ± 0.05*	0.42 ± 0.02*
LV mass (mg)	128.9 ± 5.0	168.9 ± 8.4*	157.2 ± 11.2*	95.9 ± 3.6**	128.9 ± 20.1 *,***	120.5 ± 10.9***
Ao vel. (m/s)	–	3.82 ± 0.34	2.68 ± 0.19	–	3.39 ± 0.44	2.68 ± 0.24

*P < 0.05 compared to pre-op measure in the same genotype. **P < 0.05 compared to pre-op measure of other genotype. ***P < 0.05 compared to post-op measure of other genotype.

Table 2. Echocardiographic parameters in *Aqp1*$^{+/+}$ and *Aqp1*$^{-/-}$ mice submitted to osmotic minipump infusion of Ang II. Results are means ± SEM. Two-way ANOVA for repeated measures (Sidak post hoc test).

	Ang II 2 weeks			
	WT (16)		AQP1 KO (7)	
	Pre-op	2 weeks	Pre-op	2 weeks
HR (bpm)	388 ± 8	464 ± 8*	420 ± 12**	449 ± 10
LVEDv (μl)	62.8 ± 2.4	34.6 ± 3.0*	49.6 ± 2.2**	37.9 ± 1.8*
LVESv (μl)	29.7 ± 1.7	15.1 ± 1.8*	17.7 ± 1.3**	16.0 ± 1.6
EF (%) B-mode	52.7 ± 1.8	57.3 ± 2.2	64.6 ± 2.1**	58.2 ± 2.7
IVSd (mm)	0.82 ± 0.02	1.06 ± 0.05*	0.71 ± 0.03	0.84 ± 0.04*,***
LVIDd (mm)	3.99 ± 0.06	3.09 ± 0.11*	3.64 ± 0.07**	3.31 ± 0.07*
PWd (mm)	0.84 ± 0.03	1.20 ± 0.07*	0.72 ± 0.03	0.92 ± 0.05*,***
FS (%) M-mode	26.9 ± 1.2	36.2 ± 2.0*	35.5 ± 1.7**	31.5 ± 1.7
RWT	0.42 ± 0.01	0.77 ± 0.06*	0.39 ± 0.02	0.54 ± 0.03***
LV mass (mg)	123.6 ± 3.7	129.6 ± 5.2	86.1 ± 4.5**	99.1 ± 4.6***

*P < 0.05 compared to pre-op measure of the same genotype. **P < 0.05 compared to pre-op measure of other genotype. ***P < 0.05 compared to post-op measure of other genotype.

phosphorylation was attenuated upon coincubation of myocytes with extracellular catalase (Fig. 5C). Increases in the phosphorylated active form of both ERK and p38-MAPK were similarly abrogated in myocytes from *Aqp1*$^{-/-}$ myocytes (Fig. 5, D to G). Together, these data show that agonist-induced hypertrophy requires AQP1, NOX, and the extracellular production of H_2O_2 to activate oxidant-sensitive kinases.

Facilitated transport of hydrogen peroxide in cardiac myocytes by AQP1

In addition to water, H_2O_2 permeates specific plant and eukaryotic AQPs, known as peroxiporins (*11*). To more directly examine the ability of AQP1 to facilitate the transmembrane transport of extracellular H_2O_2, intracellular H_2O_2 was measured in cardiac myocytes from *Aqp*$^{+/+}$ and *Aqp1*$^{-/-}$ mice after exposure to extracellular H_2O_2.

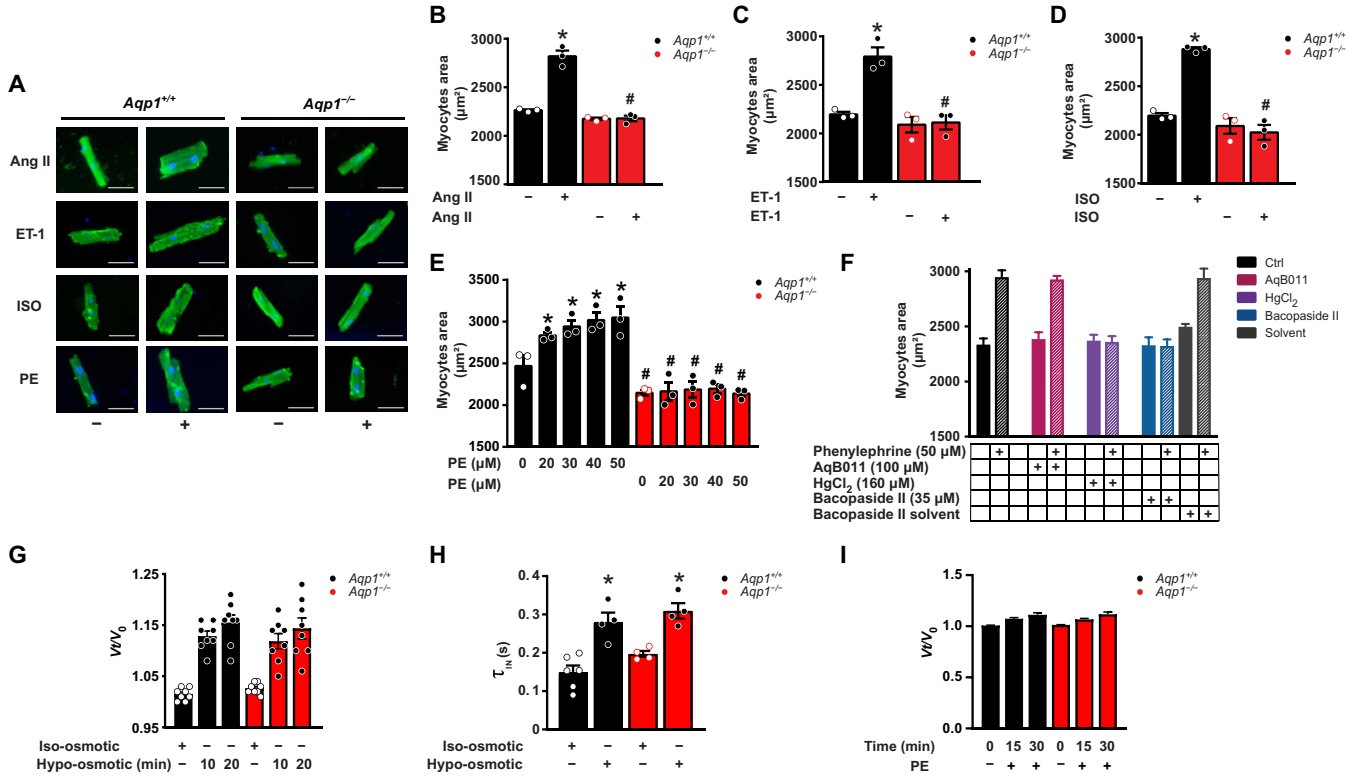

Fig. 3. The intrasubunit pore, but not the central channel, of AQP1 is necessary for hypertrophy, but not for rapid water movements in cardiac myocytes. (**A**) Representative microscopic images of single adult cardiac myocytes from *Aqp1*$^{+/+}$ and *Aqp1*$^{-/-}$ mice exposed in vitro to Ang II, endothelin-1 (ET-1), isoproterenol (ISO), phenylephrine (PE), or physiological solution for 18 hours and stained for sarcomeric α-actinin for cell surface measurements. Scale bars, 30 μM. (**B** to **E**) Cell surface area of cardiac myocytes treated with Ang II (B), ET-1 (C), ISO (D), or PE (E) (20 to 50 μM). Each dot is a mean of 30 to 70 cells per culture per condition, from independent preparations; *N* = 3 animals from each genotype. (**F**) Comparative effects of AqB011 (central channel inhibitor), $HgCl_2$, and Bacopaside II (both blockers of the intrasubunit water channel) on the prohypertrophic effect of PE in isolated cardiac myocytes cultured as above. Means ± SEM of 30 to 70 cells per culture per condition from independent preparations; *N* = 5 animals from each genotype. **P* < 0.05 compared to solvent-treated *Aqp1*$^{+/+}$ and #*P* < 0.05 compared to agonist-treated *Aqp1*$^{+/+}$ by two-way ANOVA, followed by Tukey correction for multiple testing except (F) in one-way ANOVA compared to solvent-treated *Aqp1*$^{+/+}$. (**G**) Comparative increase in cell volume (Vt/V_0) of *Aqp1*$^{+/+}$ and *Aqp1*$^{-/-}$ myocytes (*n* = 8 *Aqp1*$^{+/+}$ and 8 *Aqp1*$^{-/-}$ myocytes from two independent preparations) exposed to hypo-osmotic (100 mOsm/liter) buffer, measured by confocal fluorescence microscopy. (**H**) Comparative increase in water residence time (τ_{in}) under hypo-osmotic stress (100 mOsm/liter) in *Aqp1*$^{+/+}$ and *Aqp1*$^{-/-}$ myocyte preparations (from *N* = 6 and 4 *Aqp1*$^{+/+}$ mice under iso-osmotic or hypo-osmotic condition, respectively; *N* = 4 *Aqp1*$^{-/-}$ mice under both conditions) measured by ^{1}H-NMR relaxometry. (**I**) Comparative increase in cell volume (Vt/V_0) of *Aqp1*$^{+/+}$ and *Aqp1*$^{-/-}$ myocytes (*n* = 14 and 16 from three *Aqp1*$^{+/+}$ and four *Aqp1*$^{-/-}$ mice, respectively) exposed to phenylephrine (50 μM). (G to I) Means ± SEM; *P* < 0.05 compared to iso-osmotic or control condition in each genotype; no difference between genotypes by two-way ANOVA with Sidak correction for multiple comparisons.

To this end, cardiac myocytes were loaded with the fluorescent ROS tracer, dichlorofluorescein diacetate (DCFDA), and fluorescence monitored after exposure to H_2O_2 at different concentrations. The time-dependent increase in the fluorescent signal was attenuated in *Aqp1*$^{-/-}$ myocytes exposed to 50 or 100 μM extracellular H_2O_2, compared to *Aqp1*$^{+/+}$ myocytes (Fig. 6, A and B). To verify the identity of the oxidant species as H_2O_2 and its subcellular confinement at the plasma membrane, we repeated experiments in cardiac myocytes from *Aqp1*$^{+/+}$ and *Aqp1*$^{-/-}$ mice that had been infected with a cardiotropic recombinant adeno-associated virus type 9 (AAV9) coding for the H_2O_2-specific HyPer-3 fluorescent biosensor fused to a caveolae-targeting peptide [derived from the caveolin-interacting sequence of the endothelial nitric oxide synthase (eNOS) (*30*); Fig. 6C]. Application of H_2O_2 induced an increase in the fluorescent signal in cardiac myocytes expressing the HyPer probe. No such change in fluorescence was observed in cardiac myocytes infected with an AAV9 coding for the H_2O_2-insensitive probe, SypHer2, which was used as a negative control for the HyPer probe. The concentration-dependent increase in H_2O_2-specific fluorescent signal was substantially attenuated in *Aqp1*$^{-/-}$ myocytes compared to *Aqp1*$^{+/+}$ controls (Fig. 6C). Moreover, the increase in fluorescent signal observed in *Aqp1*$^{+/+}$ myocytes exposed to extracellular H_2O_2 was also dose-dependently attenuated by preincubation with Bacopaside II (Fig. 6D), confirming the involvement of the AQP1 water pore in the facilitated transport of H_2O_2. Stimulation of adult cardiac myocytes with phenylephrine (at concentrations that produce hypertrophy) also increased fluorescence in *Aqp1*$^{+/+}$ myocytes but not in *Aqp1*$^{-/-}$ myocytes (Fig. 6, E and F). Together, these data clearly point to a facilitated transport of H_2O_2 by the water pore of plasma membrane–localized AQP1, a process that is necessary for the hypertrophic response of cardiac myocytes.

Aqp1-dependent induction of profibrotic genes in cardiac myocytes

To gain further insight into the mechanism of regulation of cardiac fibrosis by AQP1, we measured the expression of genes coding for mediators of fibrosis that are known to be sensitive

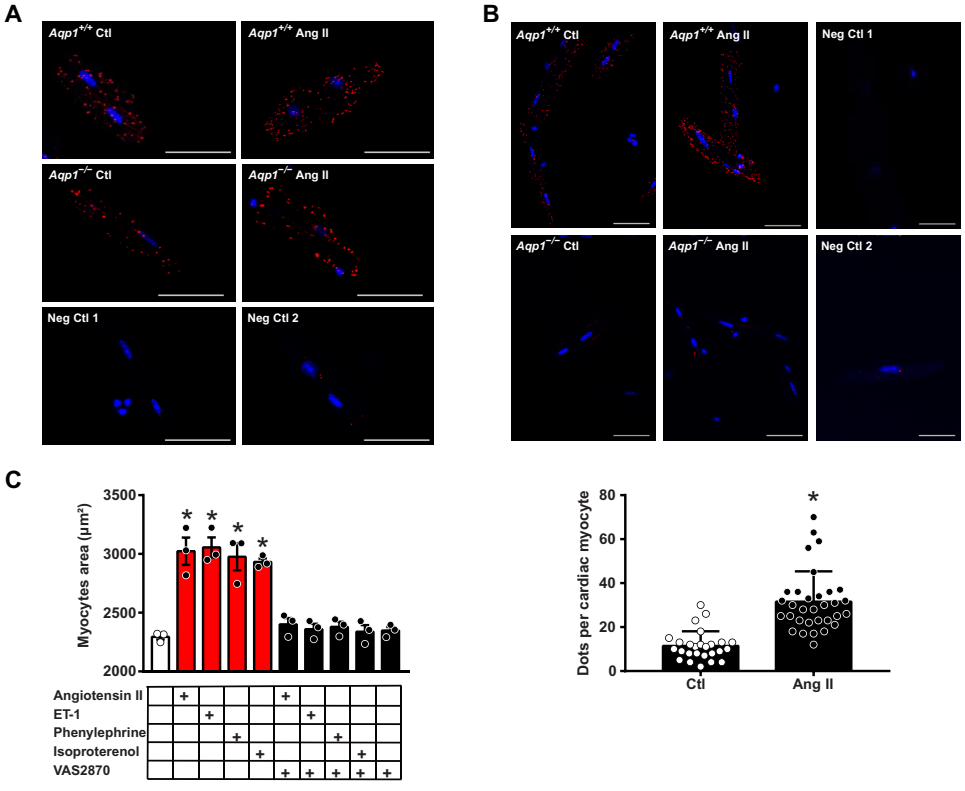

Fig. 4. NOX2-p47^{phox} colocalizes with AQP1 at the plasma membrane and mediates cardiac myocyte hypertrophy upon stimulation with Ang II. (**A**) Representative images of proximity ligation assay (PLA) showing colocalization of p47^{phox} and caveolin-3 (CAV3) at the membrane of adult cardiac myocytes from *Aqp1*$^{+/+}$ and *Aqp1*$^{-/-}$ mice, with or without Ang II (1 μM). PLA was performed 30 min after Ang II addition. Note that the deletion of AQP1 does not prevent the recruitment of p47^{phox} upon Ang II treatment. Neg Ctl 1, absence of PLA signal after omission of anti-p47^{phox} primary Ab; Neg Ctl 2, absence of PLA signal after omission of anti-CAV3 primary Ab. Scale bars, 50 μM. The experiment was repeated in three different preparations with similar results ($N = 3$). (**B**) Top: Representative image of PLA showing colocalization of p47^{phox} and AQP1 in adult cardiac myocytes from *Aqp1*$^{+/+}$ mice treated or not with Ang II (1 μM). PLA was performed 30 min after Ang II. Scale bars, 50 μM. Negative controls in *Aqp1*$^{-/-}$ myocytes (Neg Ctl 1) or *Aqp1*$^{+/+}$ myocytes incubated with secondary antibodies (but in absence of one of the primary antibodies; Neg Ctl 2) are shown in parallel. Bottom: Quantification of PLA expressed in dots per cardiac myocyte in *Aqp1*$^{+/+}$ myocytes, from independent preparations. Means ± SEM; $N = 3$. *$P < 0.05$ by Mann-Whitney test. (**C**) Effect of VAS2870, a pan-NOX inhibitor [at 0.77 μM, i.e., half-maximal inhibitory concentration for NOX2 inhibition] incubated for 18 hours on the hypertrophic response of adult cardiac myocytes from *Aqp1*$^{+/+}$ mice exposed to prohypertrophic agonists (in vitro, 18 hours). Each dot is mean cell surface area from 30 to 70 cells per culture per condition from independent preparations. Means ± SEM; $N = 3$ *Aqp1*$^{+/+}$ mice. *$P < 0.05$ compared to Ctl by one-way ANOVA, followed by Dunnett's correction for multiple comparisons.

Permeability of human AQP1 to hydrogen peroxide

To examine the permeability of human AQP1 to H_2O_2, we first aligned its protein sequence and structure with those of *Mus musculus* AQP1 (studied in our experiments above), *Rattus norvegicus* AQP1, and *Homo sapiens* AQP8 (a known "peroxiporin"), the pore sequence of which was included as positive control (fig. S5). The sequence of *H. sapiens* AQP4 was used as negative control, based on its inability to transport H_2O_2 (*32*). Residues lining the pore region, e.g., the aromatic/arginine filter region at the extracellular entrance of the pore known to be critical for filter specificity, are identical between mouse, rat, and human AQP1, as shown in Fig. 7A. In human AQP8, the key amino acids are conserved, but they are located at different positions along the sequence and in the deduced structure. More precisely, the pore residues comprise a sulfur-containing cysteine residue (Cys^{189} in AQP1 and Cys^{53} in AQP8) in the vicinity of an arginine (Arg^{195} in AQP1 and Arg^{213} in AQP8), a histidine (His^{180} in AQP1 and His^{72} in AQP8), and aromatic phenylalanine residues (Phe^{56} and Phe^{24} in AQP1 and Phe^{48} in AQP8); AQP8 contains two additional sulfur-containing residues (Cys^{208} and Met^{209}). The negative control AQP4 shows some similarity to AQP8 but lacks the two cysteines, which are replaced by a leucine (Leu^{53}) and a serine (Ser^{211}). Analysis of the interresidue interactions in AQP1 reveals that Cys^{189} makes polar interactions with Arg^{195}, as well as a sulfur-His interaction with His^{180}, which makes a His-π interaction with Phe^{56}. The latter, in turn, makes a cation-π interaction with Arg^{195} and a π-π interaction with Phe^{24} (Fig. 7A). Similar interactions are identified in rat (identical to mouse) AQP1, as well as in human AQP8 (albeit involving residues at different spatial and sequence positions; see Fig. 7A and fig. S5). Conversely, AQP4 exhibits no cysteine residue in contact with the pore, only a methionine that forms a sulfur-His interaction (Met^{212}-His^{201}), and no sulfur-Arg contact. This structural analysis supports AQP1 permeability to H_2O_2, akin to the peroxiporin AQP8.

To test this hypothesis, we explored the effect of Bacopaside II on the DCFDA fluorescence signal of human erythrocytes (with known high membrane expression of AQP1) exposed to extracellular H_2O_2 (Fig. 7B). Exposure to H_2O_2 dose-dependently increased fluorescence in untreated erythrocytes. By contrast, pretreatment with Bacopaside II strongly decreased the fluorescence induced by exposure to H_2O_2, showing that native human AQP1 also facilitates the transport of H_2O_2 across erythrocyte membranes through its water channel.

to oxidant stress in isolated cardiac myocytes (*31*). Upon stimulation with phenylephrine, the abundance of transcripts for *Tgfb2* and *Ctgf*, two major cytokines involved in the paracrine activation of fibroblasts, was clearly attenuated in cardiac myocytes isolated from *Aqp1*$^{-/-}$ mice compared to *Aqp1*$^{+/+}$ controls (fig. S4, A and B). Moreover, when cardiac fibroblasts cultured separately were incubated with medium conditioned by phenylephrine-treated primary cardiac myocytes from the two genotypes, we observed a reduction of COL1A1 protein expression, as well as of smooth muscle actin, alpha-2 (ACTA2), indicative of reduced myofibroblast differentiation, in fibroblasts exposed to the secretome of *Aqp1*$^{-/-}$ myocytes compared to *Aqp1*$^{+/+}$ controls (fig. S4, C to F). Therefore, in addition to regulating hypertrophy, AQP1 modulates cardiac myocyte production of profibrotic mediators acting on cardiac fibroblasts in a paracrine fashion.

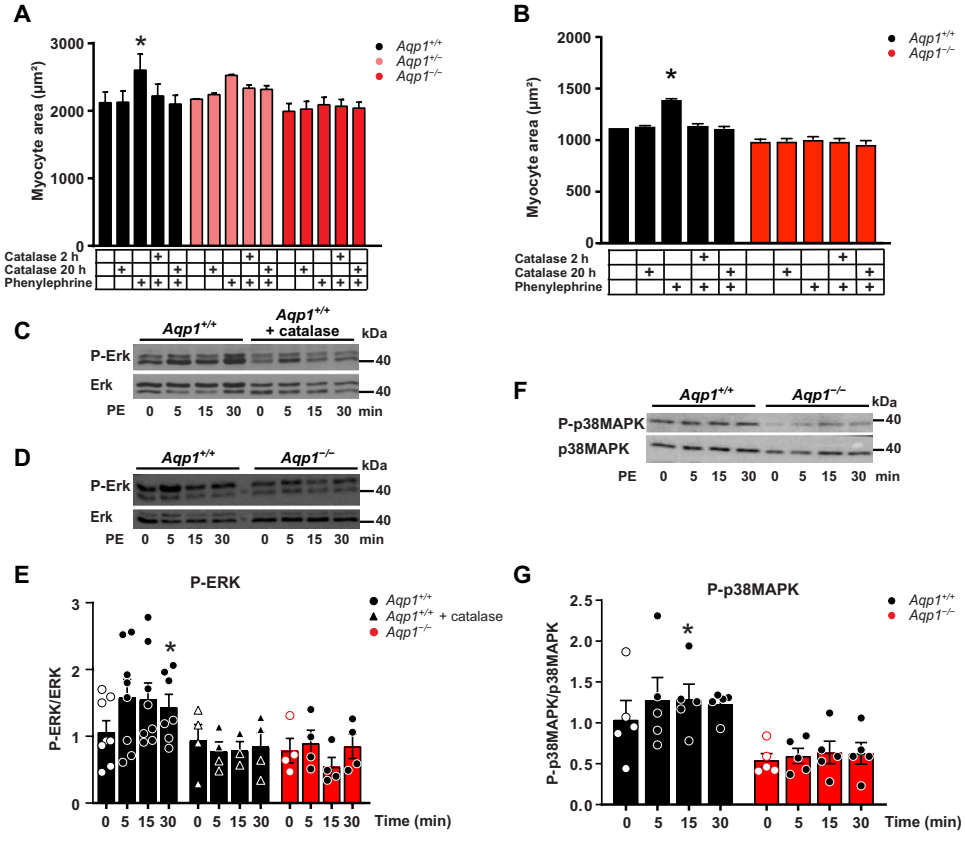

Fig. 5. AQP1 modulates the prohypertrophic signaling mediated by extracellular H_2O_2. (**A** and **B**) Effect of extracellular (non-PEGylated) catalase (incubated for 2 or 20 hours) on the hypertrophic response of cultured adult (A) or neonatal (B) murine cardiac myocytes to phenylephrine (in vitro, 18 hours). Means ± SEM of 30 to 70 cells per condition per mouse. (A) $N = 4$ adult $Aqp1^{+/+}$ and $Aqp1^{-/-}$ mice each and $N = 3$ $Aqp1^{+/-}$ mice. (B) $N = 3$ preparations from each genotype. *$P < 0.05$ by two-way ANOVA, followed by Tukey's correction for multiple comparisons. (**C** to **E**) Comparative time-dependent phospho-immunoblotted signals for P-ERK (C and D) in membrane protein extracts from isolated adult cardiac myocytes from $Aqp1^{+/+}$ mice with or without incubation with extracellular catalase (C) or from $Aqp1^{-/-}$ mice (D), exposed in vitro to PE, (C and D) representative phosphoblots, and (E) densitometric data. Means ± SEM; $N = 8$ preparations from $Aqp1^{+/+}$, $N = 4$ from $Aqp1^{+/+}$ with catalase, and $N = 4$ from $Aqp1^{-/-}$ mice. *$P < 0.05$ compared to time 0 by one-way ANOVA, followed by Dunnett's test for multiple comparisons. (**F** and **G**) Comparative time-dependent phospho-immunoblotted signals for P-p38MAPK in membrane protein extracts from isolated adult cardiac myocytes from $Aqp1^{+/+}$ or $Aqp1^{-/-}$ mice, exposed in vitro to PE. (F) Representative phosphoblot and (G) densitometric data. Means ± SEM; $N = 5$ mice from each genotype.*$P < 0.05$ compared to time 0 by one-way ANOVA, followed by Dunnett's test for multiple comparisons.

Expression of AQP1 in human induced pluripotent stem cell–derived engineered heart muscle and regulation of hypertrophy

We next used human induced pluripotent stem cell (iPSC)–derived engineered heart muscle (EHM) (*33*) to confirm the role of AQP1 in hypertrophy of human cardiac myocytes. Upon their differentiation into EHM, iPSCs increase their expression of *AQP1* to a level similar to that observed in human adult cardiac muscle (Fig. 7C). Differentiated EHM was treated with norepinephrine for 1 week with or without Bacopaside II (10 µM). The size of cardiac myocytes dissociated from the EHM was then measured using a validated flow cytometry assay as described previously (*33*). Although norepinephrine produced hypertrophy in the solvent-treated control myocytes, the response was attenuated when Bacopaside II was coapplied (Fig. 7D). Additional parameters of contractility [e.g., force-frequency relationship (Fig. 7E) and contraction/relaxation times (fig. S6)] were unaffected by AQP1 blockade.

Attenuated hypertrophy by pharmacologic blockade of AQP1 in vivo

To determine the applicability of AQP1 blockade as a strategy to block the hypertrophic response in vivo, we tested the effect of a standardized extract of the dried plant *Bacopa monnieri* in a pharmaceutical compound that is available for clinical use (KeenMind) (*34*) on Ang II–induced hypertrophy. This compound contains about 30% by weight of mixed bacosides, including Bacopaside II (~3% by weight) (*35*). We used a *Xenopus* oocyte expression system to first confirm the efficacy of the *Bacopa* extract (BE) to block human AQP1-mediated osmotic water permeability (Fig. 8, A to C). AQP1-expressing oocytes incubated in saline vehicle showed a robust swelling response as a function of time in 50% hypotonic media, whereas oocytes incubated in BE showed a reduction in the swelling rates (Fig. 8A). The dose causing half-maximal block was about 290 µg/ml of BE (Fig. 8B), corresponding roughly to 9.4 µM Bacopaside II. Trend plots comparing paired swelling rates for each AQP1-expressing oocyte in a first and second swellings assays (Fig. 8C and fig. S7) show that incubation in vehicle saline did not appreciably affect the second swelling response, in contrast to consistent decreases in swelling rate seen after incubation in increasing doses of BE. The inhibitory effect of BE was statistically significant ($P < 0.05$) at the two higher doses tested (Fig. 8C), with the highest corresponding to about 15 µM Bacopaside II. This concentration is in line with the efficient inhibitory concentration of pure Bacopaside II (20 µM) observed in parallel in the same assay (Fig. 8C), as well as on H_2O_2 permeability and hypertrophy in mouse and human cardiac myocytes.

Last, we tested the efficacy of AQP1 inhibition on the development of hypertrophy in vivo by giving BE in the food of mice submitted to minipump infusion of Ang II. On the basis of previous pharmacokinetic/pharmacodynamic data in rodents, BE was given at 1600 and 2400 mg/kg of body weight 1 week before and during the 14 days of infusion of Ang II until euthanasia. BE alone had no effect on cardiac morphometric indexes in saline-treated mice. In control mice, Ang II infusion reproduced the hypertrophic response as observed previously, but we found that cotreatment with BE dose-dependently attenuated the hypertrophic remodeling, measured as the ventricular mass (Fig. 8D) and myocyte size

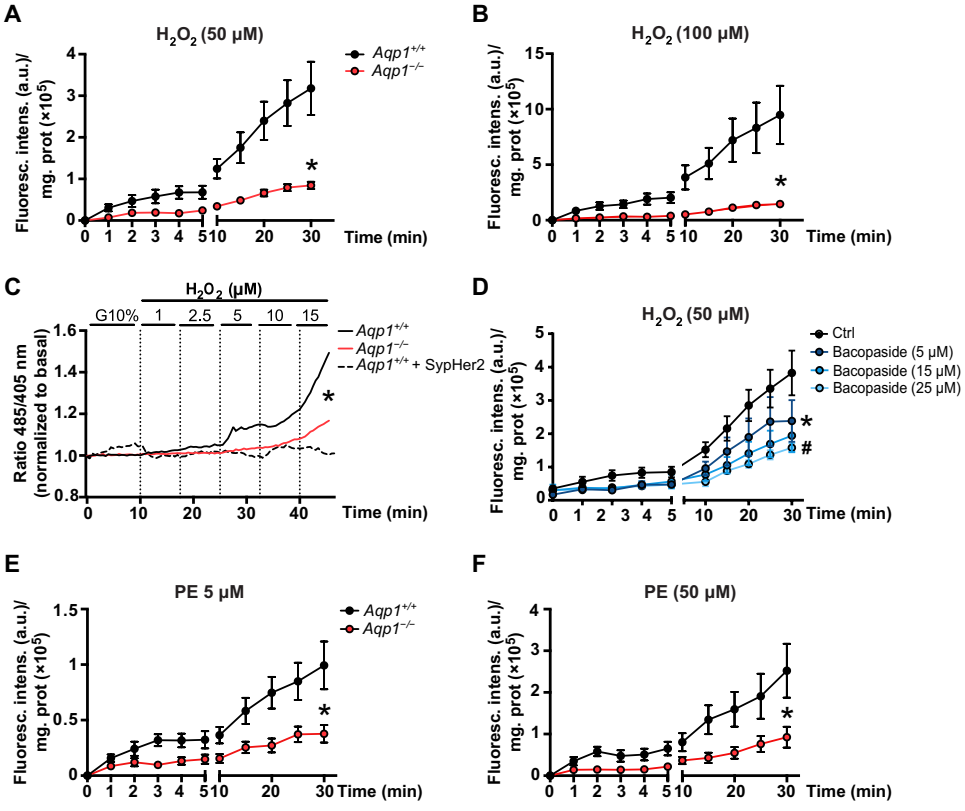

Fig. 6. AQP1 mediates the facilitated transport of H_2O_2 in mouse cardiac myocytes. (**A** and **B**) Comparative increase in intracellular reactive oxidant species (ROS; measured by DCFDA fluorescence) in isolated adult cardiac myocytes from *Aqp1*$^{+/+}$ and *Aqp1*$^{-/-}$ mice after time-dependent exposure to extracellular H_2O_2 [(A) at 50 μM and (B) at 100 μM]; independent preparations from $N = 6$ *Aqp1*$^{+/+}$ and $N = 4$ *Aqp1*$^{-/-}$ mice. (**C**) Comparative concentration-dependent increase in H_2O_2-specific HyPer-3 fluorescence ratio (measured with a caveolae-targeted sensor) in isolated adult cardiac myocytes from *Aqp1*$^{+/+}$ and *Aqp1*$^{-/-}$ mice exposed to extracellular H_2O_2. Mean of 10 cells each from $N = 6$ *Aqp1*$^{+/+}$ and $N = 6$ *Aqp1*$^{-/-}$ mice. Note the absence of signal in cardiac myocytes expressing the SyPher2 probe (insensitive to H_2O_2). (**D**) Concentration-dependent inhibitory effect of the AQP1 water channel blocker, Bacopaside II, on intracellular ROS (DCFDA fluorescence) of *Aqp1*$^{+/+}$ adult cardiac myocytes exposed to extracellular H_2O_2 (50 μM); independent preparations from $N = 4$ *Aqp1*$^{+/+}$ mice. (**E** and **F**) Comparative increase in intracellular ROS (DCFDA fluorescence) in isolated adult cardiac myocytes from *Aqp1*$^{+/+}$ and *Aqp1*$^{-/-}$ mice after time-dependent exposure to extracellular phenylephrine [(E) 5 μM and (F) 50 μM]; independent preparations from $N = 8$ *Aqp1*$^{+/+}$ and $N = 6$ *Aqp1*$^{-/-}$ mice. Means ± SEM; * or #$P < 0.05$ compared to *Aqp1*$^{+/+}$ by two-way ANOVA for repeated measures, followed by Sidak correction for multiple comparisons.

(Fig. 8E), with a more variable effect on interstitial fibrosis (Fig. 8, F and G).

DISCUSSION

We identified the water channel AQP1 as a critical modulator of the cardiac myocyte hypertrophy that is integral to myocardial remodeling that leads to heart failure. AQP1 is robustly expressed in human cardiac myocytes, and its expression correlates with the severity of cardiac hypertrophy in patients undergoing surgery to treat aortic stenosis. Genetic deletion or pharmacologic blockade of AQP1 in mouse and human iPSC-derived cardiac myocytes is sufficient to attenuate hypertrophy induced by neurohormones or hemodynamic stress. This protective effect is due to loss of transmembrane transport of H_2O_2, but not water, through the intrasubunit pore of AQP1, which is necessary for downstream hypertrophic signaling. Molecular modeling of AQP1 intrasubunit pore and functional studies in erythrocytes verified that human AQP1 mediates a similar transport of H_2O_2. Administration of standardized extracts of *B. monnieri*, containing Bacopaside inhibitors of the AQP1 intrasubunit pore, attenuated cardiac hypertrophic remodeling in mice. Together, these data support the therapeutic potential of AQP1 blockers against myocardial remodeling.

H_2O_2 has been implicated in the hypertrophic response of cardiac myocytes to a number of neurohumoral agonists and, more generally, as a signaling molecule in a wide variety of redox-regulated biological events (*36*). Multiple O_2^--producing enzymes (NOX2, NOX4, xanthine oxidoreductase, mitochondrial respiratory complexes, NOSs, and monoamine oxidases) can generate H_2O_2 after O_2^- dismutation in these cells (*37*); its subcellular distribution has been poorly characterized. In particular, NOX2 is activated by prohypertrophic agonists, but the enzyme's flavocytochrome subunit transfers electrons across the plasma membrane to produce O_2^- in the extracellular space (*28*, *38*). It had been postulated that H_2O_2 would freely diffuse back into the cell to exert downstream signaling (*39*), and we now provide evidence for facilitated H_2O_2 transport through AQP1 confined to the same subcellular compartment. Despite our use of VAS2870 at a concentration that preferentially inhibits NOX2 (*27*), note that the drug is a pan-NOX inhibitor with potential off-target effects on other isoforms, e.g., on NOX4. However, aside from the low probability of efficient inhibition of NOX4 at the concentration used here, the involvement of NOX4 is unlikely, given the cytosolic localization of this enzyme and its constitutive production of H_2O_2 intracellularly, which contrast with the stimulus dependency and sensitivity to extracellular catalase of the H_2O_2 signals observed here.

Among the 13 known AQP isoforms, AQP3 (*12*), AQP8 (*13*), and AQP9 (*14*) have also been proposed to transport H_2O_2 in heterologous expression systems, akin to specific isoforms of plant AQPs (*11*). The role of human AQP1 in the facilitated transport of H_2O_2 had not been tested in cells endogenously expressing the native protein.

Structural analysis of human AQP1 supports its ability to transport H_2O_2 and water. The diameter of H_2O_2 relative to H_2O, its neutral charge at physiological pH, and its dipole moment all are compatible with AQP1 permeation by H_2O_2 (*40*). Our analysis of the lining of amino acid side chains surrounding the extracellular entrance of the pore reveals the presence of a conserved thiol group (in Cys^{189} of AQP1), aromatic residues (Phe^{56} and Phe^{24}), a histidine

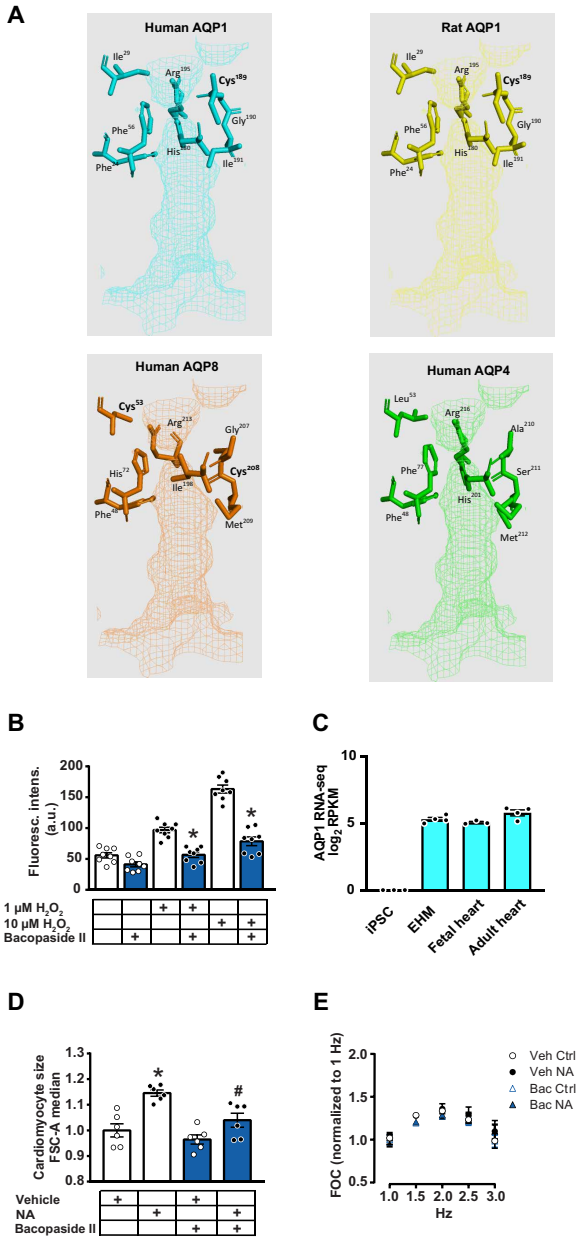

Fig. 7. Human AQP1 transports H_2O_2 and regulates the hypertrophy of human cardiac myocytes. (**A**) Graphical representation of the pore in human AQP1, rat AQP1 (modeled with 4csk as template), human AQP8 (modeled with 5i32 as template), and human AQP4: Critical residues lining the pore of the water channel are represented (see the main text for details). (**B**) Inhibition of H_2O_2-induced fluorescence increase in human AQP1-expressing erythrocytes by the AQP1 water channel blocker, Bacopaside II. DCFDA-loaded human erythrocytes were exposed to extracellular H_2O_2 and fluorescence measured by fluorescence-activated cell sorting (FACS). Means ± SEM; $N = 8$ volunteers. $^*P < 0.05$ compared to each control group without Bacopaside II (two-way ANOVA with Tukey correction for multiple comparisons). (**C**) Comparative expression of *AQP1* transcripts (by RNA-seq) in human induced pluripotent stem cells (iPSCs; $N = 3$; minimal signal equated to 0), differentiated human engineered heart muscle (EHM) cells ($N = 4$), human fetal ($N = 3$), and adult heart muscle ($N = 4$). (**D**) Inhibition of noradrenaline (NA)–induced hypertrophy in human EHM by Bacopaside II. EHM were matured for 2 weeks and subsequently subjected to NA exposure for 1 week with or without Bacopaside II (10 μM); cardiac myocyte size was determined by flow cytometry after enzymatic dispersion of EHM (n = minimum of 10,000 cells counted per EHM; six EHM per condition from two separate experimental series). Means ± SEM; $^*P < 0.05$ versus vehicle; $\#P < 0.05$ versus NA-treated EHM in absence of Bacopaside, two-way ANOVA with Tukey correction for multiple comparisons. (**E**) Contractile properties of human EHM after treatments as in (D) and assessed by measurements of force-frequency relationship (Bowditch effect) upon gradual increase in frequency of electrical stimulation from 1 to 3 Hz; force of contraction (FOC) normalized to values obtained at 1 Hz for each EHM. Means ± SEM; eight EHM per condition from two separate experiments.

(His^{180}), and an arginine (Arg^{195}) allowing a network of sulfur-π, His-π, cation-π, and π-π interactions critical for protein conformation and channel conductance. Sulfur-π and cation-π interactions in the motif may protect the thiol from oxidation (*41*, *42*), whereas the conformation of the His may change according to its environment and act as a gate. This motif and orientation of aromatic residues close to the entrance of the pore bear a high degree of similarity with the peroxiporin AQP8 but are notably different in AQP4, where a missing cysteine and the absence of the sulfur-Arg-His triad may explain a different sensitivity to oxidation driving conformational changes in the channel. The propensity of the sulfur residues to be oxidized is influenced by the surrounding microenvironment. The thiol group in cysteine and the sulfide group in methionine can interact with aromatic rings of phenylalanine, tyrosine, and tryptophan in sulfur-aromatic interactions. These interactions contribute to manipulating the orientation of the aromatic rings and provide protein stability and protection against ROS. The role of sulfur aromatic interactions is likely to be important in biological processes based on the high degree of conservation across members of the same protein family (*43*). Proteins carrying motifs of tryptophan, phenylalanine, histidine, and the sulfur aromatic residues can undergo modifications of these amino acids and modification of the protein structure under the actions of ROS (*44*). Oxidation of cysteine and methionine results in modification of sulfur-aromatic interactions and is associated with the disruption of native protein conformation and alteration of function (*45*, *46*).

Changes in the interactions between sulfur-His residues may result in changes of the spatial orientation of histidine, a mechanism compatible with the gating control of the channel under H_2O_2-induced stress. A similar mechanism was proposed for the H_2O_2-induced gating of human AQP8 (*47*). The presence of any cation-π interactions in the motif surrounding the extracellular entrance of the pore may be another important protection factor against oxidation (*41*).

π-π Interactions are important for protein folding and play a role in protection from oxidation (*48*). His-π interactions are similar to cation-π interactions and play a role in the stabilization of the protein structure. Different interactions with the aromatic rings were observed between the protonated and neutral form of the histidine, with differences related to the protein's biological function (*49*).

Analysis of the amino acid composition showed high-sequence similarity between human and rat AQP1, including the residues lining the pore region. In addition, the two proteins share the same residues within the motif surrounding the extracellular entrance of the pore. Interesting results were detected in human AQP8, in which Cys^{53}, Cys^{208}, and Met^{209} belong to a motif that may play a key role in the protection of cells against ROS damage. The analysis of the sulfur-aromatic-arginine-histidine motif close to the entrance of the pore showed a very high degree of similarity between AQP1 and AQP8, in contrast to differences in the position and interactions of the equivalent motif residues in human AQP4. In AQP4, the lack of

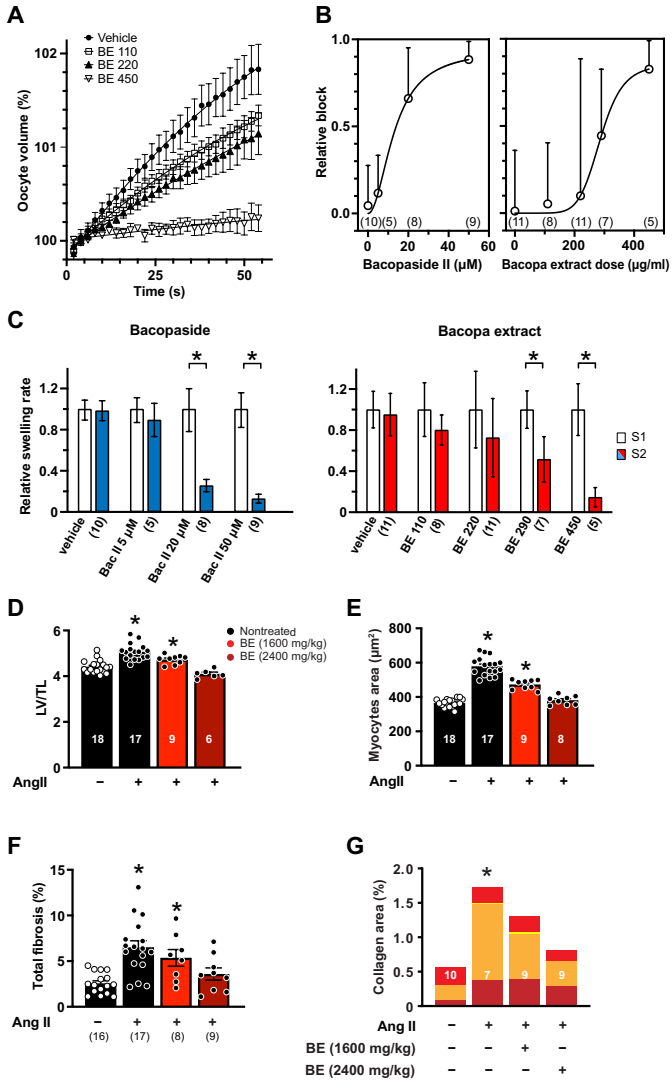

Fig. 8. A standardized extract of *B. monnieri* inhibits the intrasubunit water channel of human AQP1 and attenuates cardiac hypertrophy in vivo. (**A** to **C**) Dose-dependent inhibition by the *Bacopa* extract (BE) of osmotic water permeability in *Xenopus* oocytes expressing human AQP1 channels. (**A**) Volumes of AQP1-expressing oocytes as a function of time after introduction into 50% hypotonic saline at time 0, standardized as a percentage of the initial volume. Data are means ± SEM for $n = 4$ oocytes per treatment group. (**B**) Comparative inhibitory effects of Bacopaside II and the *Bacopa* extract, added during a second swelling assay. Relative block was calculated per oocyte from the difference in swelling rates between the first (untreated) and second hypotonic assays, divided by the rate in the first assay. Data are means ± SEM; values from (*n*) oocytes are above the *x* axis. (**C**) Histogram summary of swelling rates in the first untreated assay (S1) and the second postincubation assay (S2) conditions. Values from (*n*) oocytes are below the *x* axis; differences analyzed by ANOVA ($P < 0.0001$), and post hoc paired one-way *T* tests (*$P < 0.05$). (**D** to **G**) Oral administration of the BE attenuates Ang II-induced cardiac hypertrophy. Mice fed with the BE (1600 or 2400 mg/kg; or inactive excipient, were treated with osmotic minipump infusion of Ang II; 2 mg/kg per day) for 2 weeks and then euthanized for measurements of (**D**) left ventricle weight, normalized to tibial length. (**E**) Myocyte surface area (after WGA staining; each dot is mean from >200 myocytes per heart). (**F**) Fibrosis (Picrosirius red staining; % section area; each dot is mean from three sections per heart). (**G**) Collagen content using polarized light microscopy on Picrosirius red–stained heart sections; values from (*N*) mice as indicated in bars or below the *x* axis; *$P < 0.05$ compared to untreated Ctl, by one-way ANOVA, followed by Tukey's correction for multiple testing.

a cysteine in the motif prevents an interaction between arginine and sulfur residue, thought to be important for regulation of its reactivity (*50*), which might explain the differences in permeability to H_2O_2. Therefore, chemical and physical interaction between the cysteine, methionine, and histidine residues within this motif unique to the peroxiporins may explain protection from oxidative stress allowing permeation of the channel by H_2O_2.

Our structural analysis is supported by the presented evidence for AQP1-dependent transmembrane passage of H_2O_2 in primary mouse cardiac myocytes. The mouse is an appropriate model system, because mouse and human AQP1 are identical in amino acid composition in the pore constriction site, and we verified H_2O_2 transport in human erythrocytes. Osmotically driven rapid water transport is not affected by *Aqp1* deletion in myocytes, suggesting that AQP4, coexpressed in the same cells, compensates AQP1 loss for water movements. However, the fact that AQP4 may not transport H_2O_2 both explains the dependence on AQP1 for hypertrophy and suggests that its transport of H_2O_2, rather than water, is critical for the initiation of hypertrophic signaling. This is corroborated by the abrogation of hypertrophy with extracellular catalase. The observed colocalization of AQP1 with NOX2 and specific receptors in caveolae-enriched membrane fractions would facilitate localized signaling to effectors, such as ROS-sensitive kinases (*51*), that, in turn, relay the signal to induction of a hypertrophic response. This does not exclude the participation of cardiac AQP1 (and other AQP isoforms, e.g., AQP4) in water exchanges at later stages of tissue remodeling. Myocardial fibrosis may also result from H_2O_2 signaling in myocytes with oxidative up-regulation and paracrine release of profibrotic factors (*31*), such as transforming growth factor β2 (TGFB2) and connective tissue growth factor (CTGF) as observed here, with subsequent activation of collagen production by neighboring fibroblasts. AQP1 may also "channel" the H_2O_2 signal from other cells surrounding cardiac myocytes, such as endothelial and inflammatory cells.

Neuroendocrine stimulation, hemodynamic stress, and aging all converge to produce concentric hypertrophic remodeling, which ultimately may lead to altered diastolic (and, later, systolic) dysfunction and heart failure (*52*). Despite less concentric hypertrophy, *Aqp1*-deficient mice did not develop signs of heart failure, suggesting compensatory adaptive mechanisms. $Aqp1^{-/-}$ mice may present hypovolemia secondary to polyuria that they normally compensate with a higher water intake (*10*, *53*). However, afterload (i.e., blood pressure by telemetry and post-TAC gradients) was strictly controlled in our experimental mice. Previous studies in mice had shown that cardiac hypertrophy is dispensable to sustain the hemodynamic overload after TAC (*54*). Human EHM also maintained their contractility despite AQP1 blockade and inhibition of hypertrophy. Therefore, AQP1 inhibition may be a viable treatment of some forms of hypertrophic cardiomyopathies.

Our use of the *B. monnieri* extract (KeenMind) with its newly validated inhibitory effects on the human AQP1 intrasubunit channel extends the applicability and efficacy of this pharmacological approach in vivo. Extract of the water hyssop *B. monnieri* (also known as brahmi) is an ancient Ayurvedic remedy used to improve memory and treat anxiety and depression (*55*). A meta-analysis of human clinical studies in which *B. monnieri* was administered over several months indicated improvements in response time, attention, and possibly memory (*56*). Serious adverse events were not noted; lesser side effects included dry mouth and diarrhea. Previous randomized

and controlled clinical trials with the same BE had established its efficacy to improve the course of several neurodegenerative diseases associated with increased oxidant stress, although a mechanistic connection with AQP1 had not been identified (*57*). Beneficial outcomes ascribed to brahmi are consistent with the block of AQP1 channels as being one of the potential mechanisms of action, but additional effects on other targets are likely, due to the complexity of the Bacopaside molecule. Bacopasides administered in vivo are thought to exert effects via diverse metabolites and the original structures.

We chose the BE rather than Bacopaside II in our experiments due to cost/availability of the pure extract. Bacopaside II was shown to reversibly block AQP1, but not AQP4 water channel activity, without cytotoxicity (*23*). In silico docking based on the structure for human AQP1 [Protein Data Bank (PDB) ID: 1FQY; available at National Center for Biotechnology Information Structure] indicated an energetically favored binding site (−9.3 kcal/mol) that allowed Bacopaside II to effectively occlude the intrasubunit water pore (*23*). Polar sugar groups of the Bacopaside II molecule appeared to nest well into the intracellular vestibule of the AQP1 (but not AQP4) water pore (fig. S8). Candidate AQP1 residues in the binding pocket might include serine-71 and tyrosine-97, but these remain to be confirmed (*23*). Bacopaside II is classified as a triterpene glycoside, characterized by a hydrophobic terpene structure presumed to facilitate transmembrane entry, and three linked saccharides (arabinofuranosyl-glucopyranosyl-glucopyranoside) that appear to serve as the AQP1-binding ligand (fig. S8B). AQP1 water channel activity showed half-maximal block after 0.5-hour preincubation with Bacopaside II and maximum block by 1.3 hours (*23*). Other AQP1 ligands such as AqB013, AqB011, and AqF026 also are postulated to bind intracellularly (*22*, *58*, *59*) and have similarly slow rates for the onset of block, supporting the proposed intracellular site of action for Bacopaside II. Theoretical considerations note shortcomings of Bacopaside II as a therapeutic agent in that it exceeds Lipinski's Rule of Five limits for size, hydrophobicity, and hydrogen bond sites. However, using Bacopaside II as a lead compound, ongoing work is exploring polysaccharides as possible endogenous modulators of AQP channels, which could offer new lines of therapeutics not previously considered.

Despite our observation of an antihypertrophic effect of Bacopaside in mice and iPSC-derived human cardiac myocytes, similar protective properties against myocardial remodeling remain to be demonstrated in patients. This can be prospectively tested with this low-cost, standardized, and clinically available extract. Together, our studies open the way to complement the therapeutic armamentarium with specific blockers of AQP1 for the prevention of adverse remodeling in cardiovascular diseases leading to heart failure.

MATERIALS AND METHODS

Study design

We tested the hypothesis that AQP1 regulates myocardial remodeling by controlling the plasmalemmal transport of H_2O_2 in cardiac myocytes. We compared the hypertrophic and fibrotic response to hemodynamic stress (transaortic constriction) and to neurohormonal stimuli in vivo by quantitative histomorphometry between *Aqp1*-deficient mice and their wild-type littermates. We used primary adult cardiac myocytes from $Aqp1^{+/+}$ and $Aqp1^{-/-}$ mice to compare their hypertrophic response to neurohormonal stimuli in vitro, as well as their transmembrane passage of H_2O_2. Similar experiments were repeated in human iPSC-derived EHM and human erythrocytes expressing native human AQP1. The effect of Bacopaside extracts that inhibit AQP1 was measured on hypertrophy and H_2O_2 transport in the same models.

The number of animals in experimental studies using adult mice was calculated on the basis of a Bayesian principle of noninformative a priori, i.e., supposing a $P = 0.5$ on the probability of an experimental response, a minimum of five animals per group need to be considered to maintain a basis of 5% on the type I error. For in vitro experiments, primary isolates were obtained from at least three independent preparations from three different animals (*N*). Cell measurements were obtained from >200 cells per animal (12 to 14 myocytes measured in each of six randomly chosen microscopic fields in each of three histological sections per heart) and 30 to 70 cells per condition (three to seven myocytes measured in each of 10 randomly taken photomicrographs from each in vitro culture). All experiments were conducted in a blinded fashion, i.e., the operators treating mice or cells, and assessing that the end points were blinded to the mouse genotype. Before unblinding, raw data were examined for normal distribution using the Shapiro-Wilk test; when outliers were identified, they were excluded from analysis if justified on the basis of confirmed technical failure in parameter acquisition. All experiments on $Aqp1^{-/-}$ mice were compared to their $Aqp1^{+/+}$ littermate controls. Individual subject-level data are reported in data files S1 and S2.

Animals

Breeding pairs of heterozygous $Aqp1^{+/-}$ mice in the Sv129 background were obtained from O. Devuyst (Division of Nephrology, UCLouvain, Belgium). Heterozygous mice were crossbred to obtain homozygous $Aqp1^{-/-}$ mice and their $Aqp1^{+/+}$ littermate controls. All studied mice were at least 16 weeks old at the time of banding and age-matched between genotypes. Experimental procedures, including aortic banding, minipump infusion of Ang II, echocardiographic, telemetry measurements, and isolation of isotypic primary cells, as well as measurements of remodeling parameters, are described in the Supplementary Materials. All protocols were carried out in accordance with the Guide for the Care and Use of Laboratory Animals published by the U.S. National Institutes of Health (NIH) and the European Directive 2010/63/EU and were approved by local ethical committees.

Oxidation of caveolae-targeted HyPer-3 by H_2O_2

Fluorescence measurements were performed with the H_2O_2-specific HyPer-3 fluorescent reporter. The first 97 amino acids of eNOSs, which are responsible for the protein's targeting to the caveolae, were fused to the N terminus of HyPer-3 with a NEBuilder HiFi DNA Assembly system (New England Biolabs). The resultant complementary DNA (cDNA) was subcloned into an AAV expression vector (StrataGene), where expression was driven by the cytomegalovirus promoter. This construct was then packaged into AAV9 viral particles by the Children's Hospital Boston Viral Vector Core. The cDNA coding the SyPher2 probe, which is insensitive to H_2O_2, was processed similarly to serve as control for the HyPer-3 probe. $Aqp1^{+/+}$ and $Aqp1^{-/-}$ mice were infected with about 5×10^{11} genome copies of virus via retro-orbital injection. After 5 weeks of infection, cardiac myocytes were isolated as described above and plated on coverslips. After a few hours or overnight culture, the coverslip was mounted

in a chamber maintained at 37°C and placed on the stage of an inverted microscope equipped with a 40× oil immersion objective. The cells were perfused at a flow rate of ~1 ml/min with a bicarbonate-buffered Krebs solution containing 120 mM NaCl, 4.8 mM KCl, 2.5 mM $CaCl_2$, 24 mM $NaHCO_3$, bovine serum albumin (1 g/liter; Fraction V, Roche), and 10 mM glucose. This solution was continuously gassed with O_2/CO_2 (94/6) to maintain the pH value around 7.4. The fluorescence ratio of HyPer-3 was measured every 30 s after double excitation, at 480 and 400 nm, using an emission filter centered at 535 nm. After 10-min perfusion, cardiac myocytes were exposed to a stepwise increase in hydrogen peroxide concentration (7.5-min steps at 1, 2.5, 5, 10, and 15 μM H_2O_2). To allow comparison between experiments and genotypes, the fluorescence ratio of each cell was normalized to the initial ratio measured during the first 2 min. After exclusion of cardiac myocytes (from *Aqp1*$^{+/+}$ or *Aqp1*$^{-/-}$ mice) that detached from the coverslip during the experiment or that displayed no HyPer-3 response to 15 μM H_2O_2 because of too low expression of the sensor, 10 of 18 cells from six *Aqp1*$^{+/+}$ mice and 10 of 14 cells from six *Aqp1*$^{-/-}$ mice were used to compute the mean trace.

Preparation of EHM from human iPSCs

Human iPSC-derived cardiac myocytes

Human cardiac myocytes were derived from the TC1133 line [lot number: 50-001-21 from LiPSC-GR1.1 line reported in (*60*)] by directed differentiation according to Tiburcy *et al.* (*33*) with slight modifications. Briefly, PSCs were plated at 1.3×10^4 cells/cm^2 on 1:120 Matrigel in phosphate-buffered saline (PBS)–coated plates and cultured in StemMACS iPS-Brew XF (Miltenyi Biotec) for 4 days. To induce cardiac differentiation, cells were rinsed with RPMI 1640 and then treated with RPMI 1640, 2% B27 minus insulin, 200 μM L-ascorbic acid-2-phosphate sesquimagnesium salt hydrate (Sigma-Aldrich), activin A (9 ng/ml; R&D Systems), bone morphogenetic protein 4 (5 ng/ml; R&D Systems), 1 μM CHIR99021 (Stemgent), and fibroblast growth factor–2 (FGF-2; 5 ng/ml; PeproTech) for 3 days. After another wash with RPMI 1640, cells were cultured from days 4 to 10 with 5 μM inhibitor of Wnt production-4 (IWP4) (Stemgent), followed by RPMI 1640, 2% B27, and 200 μM L-ascorbic acid-2-phosphate sesquimagnesium. Cardiac myocytes were metabolically purified by glucose deprivation from days 13 to 17 in RPMI 1640 without glucose (Thermo Fisher Scientific), 2.2 mM sodium lactate (Sigma-Aldrich), 100 μM β-mercaptoethanol (Sigma-Aldrich), penicillin (100 U/ml), and streptomycin (100 μg/ml).

EHM generation

Defined, serum-free EHM was generated from high-purity cardiomyocytes (>95% actinin$^+$) and human foreskin fibroblasts (American Type Culture Collection) at a 70:30% ratio as previously described (*33*). The cells were reconstituted in a mixture of pH-neutralized medical grade bovine collagen (LLC Collagen Solutions; 0.4 mg per EHM), concentrated serum-free medium [2× RPMI 1640, 8% B27 without insulin, penicillin (200 U/ml), and streptomycin (200 μg/ml)], and cultured for 3 days in Iscove medium with 4% B27 without insulin, 1% nonessential amino acids, 2 mM glutamine, 300 μM ascorbic acid, insulin-like growth factor 1 (100 ng/ml; AF-100-11), FGF-2 (10 ng/ml; AF-100-18B), vascular endothelial growth factor 165 (5 ng/ml; AF-100-20), TGF-β1 (5 ng/ml; AF-100-21C; all growth factors are from PeproTech), penicillin (100 U/ml), and streptomycin (100 μg/ml). After a 3-day condensation period, EHM were transferred to flexible holders for auxotonic loading and cardiomyocyte maturation as previously described (*61*). Treatment with L-norepinephrine hydrochloride (Sigma-Aldrich; prepared in distilled water containing 200 μM L-ascorbic acid-2-phosphate sesquimagnesium salt hydrate) and Bacopaside II (Sigma-Aldrich; 10 mM stock prepared in methanol) was initiated on week 3 of EHM maturation. EHMs were treated with indicated concentrations for 7 days.

Analysis of contractile function

Contraction experiments were performed under isometric conditions in organ baths at 37°C in gassed (5% CO_2/95% O_2) Tyrode's solution (containing 120 mM NaCl, 1 mM $MgCl_2$, 0.2 mM $CaCl_2$, 5.4 mM KCl, 22.6 mM $NaHCO_3$, 4.2 mM NaH_2PO_4, 5.6 mM glucose, and 0.56 mM ascorbate). EHMs were electrically stimulated at 1.5 Hz with 5-ms square pulses of 200 mA. EHMs were mechanically stretched at intervals of 125 μm until the maximum systolic force amplitude [force of contraction (FOC)] was observed according to the Frank-Starling law. Force-frequency measurements were performed at half-maximal effective concentration calcium concentrations determined individually for each EHM.

Flow cytometry hypertrophy assay

EHMs were digested in collagenase 1 solution (2 mg/ml in calcium-containing PBS in the presence of 20% fetal bovine serum) at 37°C for 90 min. EHMs were then washed with PBS (without calcium) and further incubated in Accutase (Millipore), 0.0125% Trypsin (Life Technologies), and deoxyribonuclease (20 μg/ml; Calbiochem) for 30 min at room temperature. Cells were then mechanically separated, and single-cell suspensions were obtained by passing the cells through a 70-μm cell strainer. Cell were fixed in with 70% ice-cold ethanol and stained for sarcomeric α-actinin (Sigma-Aldrich) and Hoechst-3342 (10 μg/ml; Life Technologies). The following gating strategy was applied, as described previously (*33*), to assess cardiac myocyte volume: (i) gating of cells based on forward scatter area (FSC-A) and sideward scatter area, (ii) gating of live cells (nuclear DNA content), (iii) gating of single cells (based on DNA signal width), (iv) gating of actinin$^+$ cardiac myocytes, and (v) assessment of cardiac myocyte size based on median FSC-A. Cells were run on the LSRII SORP Cytometer (BD Biosciences) and analyzed using DIVA software. At least 10,000 live cells were analyzed per sample.

Myocardial samples from patients

Human endomyocardial biopsies from patients with aortic stenosis were obtained during surgery from patients suffering of aortic stenosis ($n = 26$) in accordance with the local ethics committee (Comité éthique hospitalo-facultaire des Cliniques Universitaires St Luc, Brussels, Belgium) with signed informed consent obtained before surgery. Cardiac biopsies were immediately frozen in liquid nitrogen and stored at −80°C. For cardiac myocyte–isolated nuclei, human heart specimens from hypertrophic and healthy myocardial tissue were provided by the Department of Forensic Medicine in Stockholm, Sweden. Ethical permissions were obtained from local ethical committees. Individual patient details are listed in table S1. All procedures for immunohistochemistry, cardiac myocyte nuclear isolation, and RNA analysis are described in the Supplementary Materials.

Structural analysis of AQPs

The sequence and structure of the target AQP (P29972, PDB code 4CSK) were aligned with the sequence and structure of other mammalian AQPs sharing at least 40% identity with the target using PDBeFOLD (*62*). For the proteins with no experimental structure

in the PDB (*63*), the structures were modeled using the comparative modeling webserver SWISS-MODEL (*64*). Analysis of the amino acids lining the pore was performed using the web-based resource PoreWalker (*65*), whereas the analysis of solvent accessibility and that of interactions were performed for each protein structure using the MuSiC suite (*66*), Protein Interaction Calculator web server (*67*), and an in-house program (*68*). PyMOL was used as a visualization tool of the protein structure (The PyMOL Molecular Graphics System, version 2.0 Schrödinger LLC).

Statistical analysis

All results of continuous variables are expressed as means ± SEM. Raw data were first analyzed to confirm their normal distribution and then analyzed by unpaired Student's *t* test, one-way analysis of variance (ANOVA), two-way ANOVA, or two-way ANOVA for repeated measures where appropriate. Dunett or Sidak correction (one-way ANOVA) and Tukey or Sidak correction (two-way ANOVA) were applied to correct for multiple comparisons. In the absence of a normal distribution, a nonparametric Krukal-Wallis or Mann-Whitney test were used, followed by Dunn's correction for multiple comparisons if appropriate. $P < 0.05$ was considered statistically significant.

SUPPLEMENTARY MATERIALS

stm.sciencemag.org/cgi/content/full/12/564/eaay2176/DC1

Materials and Methods

Fig. S1. Expression of AQP4 in mouse cardiac myocytes and *AQP* in pericentriolar material 1–positive nuclear RNA from control and hypertrophic human myocardium.

Fig. S2. Afterload control in *Aqp1* mice under TAC or Ang II infusion and effect of endothelin-1 on [^{14}C]-phenylalanine incorporation in adult cardiac myocytes from *Aqp1*$^{+/+}$ and *Aqp1*$^{-/-}$ mice.

Fig. S3. Fluorescence-based measurements of cell water intake in adult mouse cardiac myocytes exposed to hypo-osmotic buffer.

Fig. S4. Reduced expression of profibrotic mediators in *Aqp1*$^{-/-}$ cardiac myocytes and of their paracrine effect in cardiac fibroblasts.

Fig. S5. Protein sequence alignment using AQP1 as target.

Fig. S6. Effect of Bacopaside II on contractile properties of EHM with or without noradrenaline.

Fig. S7. Inhibitory effect of the standardized extract of *B. monnieri* on AQP1-mediated water permeability in *Xenopus* oocytes.

Fig. S8. Schematic diagram summarizing the proposed mechanism of AQP1 inhibition by Bacopaside II.

Table S1. Clinical characteristics of donors with normal versus hypertrophic left ventricular remodeling.

Table S2. Sequences of primers used in RT-qPCR.

Data file S1. Individual subject-level data for main figures.

Data file S2. Individual subject-level data for supplementary figures.

References (*69*–*82*)

View/request a protocol for this paper from *Bio-protocol*.

REFERENCES AND NOTES

1. R. Knöll, G. Iaccarino, G. Tarone, D. Hilfiker-Kleiner, J. Bauersachs, A. F. Leite-Moreira, P. H. Sugden, J.-L. Balligand; European Society of Cardiology, Towards a re-definition of 'cardiac hypertrophy' through a rational characterization of left ventricular phenotypes: A position paper of the Working Group 'Myocardial Function' of the ESC. *Eur. J. Heart Fail.* **13**, 811–819 (2011).
2. A. P. Lourenco, A. F. Leite-Moreira, J.-L. Balligand, J. Bauersachs, D. Dawson, R. A. de Boer, L. J. de Windt, I. Falcão-Pires, R. Fontes-Carvalho, S. Franz, M. Giacca, D. Hilfiker-Kleiner, E. Hirsch, C. Maack, M. Mayr, B. Pieske, T. Thum, C. G. Tocchetti, D. L. Brutsaert, S. Heymans, An integrative translational approach to study heart failure with preserved ejection fraction: A position paper from the Working Group on Myocardial Function of the European Society of Cardiology. *Eur. J. Heart Fail.* **20**, 216–227 (2018).
3. Y. Ye, J. Li, Z. Yuan, Effect of antioxidant vitamin supplementation on cardiovascular outcomes: A meta-analysis of randomized controlled trials. *PLOS ONE* **8**, e56803 (2013).
4. G. Bjelakovic, D. Nikolova, L. L. Gluud, R. G. Simonetti, C. Gluud, Mortality in randomized trials of antioxidant supplements for primary and secondary prevention: Systematic review and meta-analysis. *JAMA* **297**, 842–857 (2007).
5. G. G. Schiattarella, F. Altamirano, D. Tong, K. M. French, E. Villalobos, S. Y. Kim, X. Luo, N. Jiang, H. I. May, Z. V. Wang, T. M. Hill, P. P. A. Mammen, J. Huang, D. I. Lee, V. S. Hahn, K. Sharma, D. A. Kass, S. Lavandero, T. G. Gillette, J. A. Hill, Nitrosative stress drives heart failure with preserved ejection fraction. *Nature* **568**, 351–356 (2019).
6. T. Münzel, G. G. Camici, C. Maack, N. R. Bonetti, V. Fuster, J. C. Kovacic, Impact of oxidative stress on the heart and vasculature: Part 2 of a 3-part series. *J. Am. Coll. Cardiol.* **70**, 212–229 (2017).
7. B. Steinhorn, A. Sorrentino, S. Badole, Y. Bogdanova, V. Belousov, T. Michel, Chemogenetic generation of hydrogen peroxide in the heart induces severe cardiac dysfunction. *Nat. Commun.* **9**, 4044 (2018).
8. A. Arcaro, F. Pirozzi, A. Angelini, C. Chimenti, L. Crotti, C. Giordano, D. Mancardi, D. Torella, C. G. Tocchetti, Novel perspectives in redox biology and pathophysiology of failing myocytes: Modulation of the intramyocardial redox milieu for therapeutic interventions—A review article from the working group of cardiac cell biology, Italian society of cardiology. *Oxid. Med. Cell Longev.* **2016**, 6353469 (2016).
9. P. Agre, The aquaporin water channels. *Proc. Am. Thorac. Soc.* **3**, 5–13 (2006).
10. V. Montiel, E. Leon Gomez, C. Bouzin, H. Esfahani, M. Romero Perez, I. Lobysheva, O. Devuyst, C. Dessy, J. L. Balligand, Genetic deletion of aquaporin-1 results in microcardia and low blood pressure in mouse with intact nitric oxide-dependent relaxation, but enhanced prostanoids-dependent relaxation. *Pflugers Arch.* **466**, 237–251 (2014).
11. G. P. Bienert, F. Chaumont, Aquaporin-facilitated transmembrane diffusion of hydrogen peroxide. *Biochim. Biophys. Acta* **1840**, 1596–1604 (2014).
12. E. W. Miller, B. C. Dickinson, C. J. Chang, Aquaporin-3 mediates hydrogen peroxide uptake to regulate downstream intracellular signaling. *Proc. Natl. Acad. Sci. U.S.A.* **107**, 15681–15686 (2010).
13. M. Bertolotti, S. Bestetti, J. M. García-Manteiga, I. Medraño-Fernandez, A. Dal Mas, M. L. Malosio, R. Sitia, Tyrosine kinase signal modulation: A matter of H_2O_2 membrane permeability? *Antioxid. Redox Signal.* **19**, 1447–1451 (2013).
14. S. Watanabe, C. S. Moniaga, S. Nielsen, M. Hara-Chikuma, Aquaporin-9 facilitates membrane transport of hydrogen peroxide in mammalian cells. *Biochem. Biophys. Res. Commun.* **471**, 191–197 (2016).
15. B. Yang, Y. Song, D. Zhao, A. S. Verkman, Phenotype analysis of aquaporin-8 null mice. *Am. J. Physiol. Cell Physiol.* **288**, C1161–C1170 (2005).
16. A. S. Verkman, Knock-out models reveal new aquaporin functions. *Handb. Exp. Pharmacol.* **2009**, 359–381 (2009).
17. S. Al-Samir, Y. Wang, J. D. Meissner, G. Gros, V. Endeward, Cardiac morphology and function, and blood gas transport in aquaporin-1 knockout mice. *Front. Physiol.* **7**, 181 (2016).
18. T. L. Butler, C. G. Au, B. Yang, J. R. Egan, Y. M. Tan, E. C. Hardeman, K. N. North, A. S. Verkman, D. S. Winlaw, Cardiac aquaporin expression in humans, rats, and mice. *Am. J. Physiol. Heart Circ. Physiol.* **291**, H705–H713 (2006).
19. A. O. Verkerk, E. M. Lodder, R. Wilders, Aquaporin channels in the heart—Physiology and pathophysiology. *Int. J. Mol. Sci.* **20**, 2039 (2019).
20. B. Thienpont, J. M. Aronsen, E. L. Robinson, H. Okkenhaug, E. Loche, A. Ferrini, P. Brien, K. Alkass, A. Tomasso, A. Agrawal, O. Bergmann, I. Sjaastad, W. Reik, H. L. Roderick, The H3K9 dimethyltransferases EHMT1/2 protect against pathological cardiac hypertrophy. *J. Clin. Invest.* **127**, 335–348 (2017).
21. J. Yu, A. J. Yool, K. Schulten, E. Tajkhorshid, Mechanism of gating and ion conductivity of a possible tetrameric pore in aquaporin-1. *Structure* **14**, 1411–1423 (2006).
22. M. Kourghi, J. V. Pei, M. L. De Ieso, G. Flynn, A. J. Yool, Bumetanide derivatives AqB007 and AqB011 selectively block the aquaporin-1 ion channel conductance and slow cancer cell migration. *Mol. Pharmacol.* **89**, 133–140 (2016).
23. J. V. Pei, M. Kourghi, M. L. De Ieso, E. M. Campbell, H. S. Dorward, J. E. Hardingham, A. J. Yool, Differential inhibition of water and ion channel activities of mammalian aquaporin-1 by two structurally related bacopaside compounds derived from the medicinal plant *Bacopa monnieri*. *Mol. Pharmacol.* **90**, 496–507 (2016).
24. T. Münzel, T. Gori, J. F. Keaney Jr., C. Maack, A. Daiber, Pathophysiological role of oxidative stress in systolic and diastolic heart failure and its therapeutic implications. *Eur. Heart J.* **36**, 2555–2564 (2015).
25. A. Van Steenbergen, M. Balteau, A. Ginion, L. Ferté, S. Battault, C. de Meester de Ravenstein, J.-L. Balligand, E. P. Daskalopoulos, P. Gilon, F. Despa, S. Despa, J.-L. Vanoverschelde, S. Horman, H. Koepsell, G. Berry, L. Hue, L. Bertrand, C. Beauloye, Sodium-myoinositol cotransporter-1, SMIT1, mediates the production of reactive oxygen species induced by hyperglycemia in the heart. *Sci. Rep.* **7**, 41166 (2017).
26. S. Altenhöfer, K. A. Radermacher, P. W. Kleikers, K. Wingler, H. H. Schmidt, Evolution of NADPH oxidase inhibitors: Selectivity and mechanisms for target engagement. *Antioxid. Redox Signal.* **23**, 406–427 (2015).
27. V. T.-V. Dao, M. H. Elbatreek, S. Altenhöfer, A. I. Casas, M. P. Pachado, C. T. Neullens, U. G. Knaus, H. H. Schmidt, Isoform-selective NADPH oxidase inhibitor panel for pharmacological target validation. *Free Radic. Biol. Med.* **148**, 60–69 (2020).

28. A. B. Fisher, Redox signaling across cell membranes. *Antioxid. Redox Signal.* **11**, 1349–1356 (2009).
29. K. Chen, S. E. Craige, J. F. Keaney Jr., Downstream targets and intracellular compartmentalization in Nox signaling. *Antioxid. Redox Signal.* **11**, 2467–2480 (2009).
30. H. Kalwa, J. L. Sartoretto, R. Martinelli, N. Romero, B. S. Steinhorn, M. Tao, C. K. Ozaki, C. V. Carman, T. Michel, Central role for hydrogen peroxide in P2Y1 ADP receptor-mediated cellular responses in vascular endothelium. *Proc. Natl. Acad. Sci. U.S.A.* **111**, 3383–3388 (2014).
31. N. Hermida, L. Michel, H. Esfahani, E. Dubois-Deruy, J. Hammond, C. Bouzin, A. Markl, H. Colin, A. V. Steenbergen, C. De Meester, C. Beauloye, S. Horman, X. Yin, M. Mayr, J.-L. Balligand, Cardiac myocyte β3-adrenergic receptors prevent myocardial fibrosis by modulating oxidant stress-dependent paracrine signaling. *Eur. Heart J.* **39**, 888–898 (2018).
32. G. P. Bienert, A. L. Møller, K. A. Kristiansen, A. Schulz, I. M. Møller, J. K. Schjoerring, T. P. Jahn, Specific aquaporins facilitate the diffusion of hydrogen peroxide across membranes. *J. Biol. Chem.* **282**, 1183–1192 (2007).
33. M. Tiburcy, J. E. Hudson, P. Balfanz, S. Schlick, T. Meyer, M.-L. C. Liao, E. Levent, F. Raad, S. Zeidler, E. Wingender, J. Riegler, M. Wang, J. D. Gold, I. Kehat, E. Wettwer, U. Ravens, P. Dierickx, L. W. van Laake, M. J. Goumans, S. Khadjeh, K. Toischer, G. Hasenfuss, L. A. Couture, A. Unger, W. A. Linke, T. Araki, B. Neel, G. Keller, L. Gepstein, J. C. Wu, W.-H. Zimmermann, Defined engineered human myocardium with advanced maturation for applications in heart failure modeling and repair. *Circulation* **135**, 1832–1847 (2017).
34. C. Stough, L. A. Downey, J. Lloyd, B. Silber, S. Redman, C. Hutchison, K. Wesnes, P. J. Nathan, Examining the nootropic effects of a special extract of *Bacopa monniera* on human cognitive functioning: 90 day double-blind placebo-controlled randomized trial. *Phytother. Res.* **22**, 1629–1634 (2008).
35. A. Dowell, G. Davidson, D. Ghosh, Validation of quantitative HPLC method for Bacosides in KeenMind. *Evid. Based Complement. Alternat. Med.* **2015**, 696172 (2015).
36. K. M. Holmström, T. Finkel, Cellular mechanisms and physiological consequences of redox-dependent signalling. *Nat. Rev. Mol. Cell Biol.* **15**, 411–421 (2014).
37. J. R. Burgoyne, H. Mongue-Din, P. Eaton, A. M. Shah, Redox signaling in cardiac physiology and pathology. *Circ. Res.* **111**, 1091–1106 (2012).
38. W. M. Nauseef, Detection of superoxide anion and hydrogen peroxide production by cellular NADPH oxidases. *Biochim. Biophys. Acta* **1840**, 757–767 (2014).
39. E. Schröder, P. Eaton, Hydrogen peroxide as an endogenous mediator and exogenous tool in cardiovascular research: Issues and considerations. *Curr. Opin. Pharmacol.* **8**, 153–159 (2008).
40. A. Almasalmeh, D. Krenc, B. Wu, E. Beitz, Structural determinants of the hydrogen peroxide permeability of aquaporins. *FEBS J.* **281**, 647–656 (2014).
41. D. K. Chakravorty, B. Wang, M. N. Ucisik, K. M. Merz Jr., Insight into the cation–π interaction at the metal binding site of the copper metallochaperone CusF. *J. Am. Chem. Soc.* **133**, 19330–19333 (2011).
42. K. S. C. Reid, P. F. Lindley, J. M. Thornton, Sulphur-aromatic interactions in proteins. *FEBS Lett.* **190**, 209–213 (1985).
43. R. Bhattacharyya, D. Pal, P. Chakrabarti, Disulfide bonds, their stereospecific environment and conservation in protein structures. *Protein Eng. Des. Sel.* **17**, 795–808 (2004).
44. B. A. Freeman, J. D. Crapo, Biology of disease: Free radicals and tissue injury. *Lab. Invest.* **47**, 412–426 (1982).
45. A. K. Lewis, K. M. Dunleavy, T. L. Senkow, C. Her, B. T. Horn, M. A. Jersett, R. Mahling, M. R. McCarthy, G. T. Perell, C. C. Valley, C. B. Karim, J. Gao, W. C. Pomerantz, D. D. Thomas, A. Cembran, A. Hinderliter, J. N. Sachs, Oxidation increases the strength of the methionine-aromatic interaction. *Nat. Chem. Biol.* **12**, 860–866 (2016).
46. D. Pal, P. Chakrabarti, Non-hydrogen bond interactions involving the methionine sulfur atom. *J. Biomol. Struct. Dyn.* **19**, 115–128 (2001).
47. S. Bestetti, I. Medraño-Fernandez, M. Galli, M. Ghitti, G. P. Bienert, G. Musco, A. Orsi, A. Rubartelli, R. Sitia, A persulfidation-based mechanism controls aquaporin-8 conductance. *Sci. Adv.* **4**, eaar5770 (2018).
48. K. Madhusudan Makwana, R. Mahalakshmi, Implications of aromatic–aromatic interactions: From protein structures to peptide models. *Protein Sci.* **24**, 1920–1933 (2015).
49. E. Cauët, M. Rooman, R. Wintjens, J. Liévin, C. Biot, Histidine–aromatic interactions in proteins and protein–ligand complexes: Quantum chemical study of x-ray and model structures. *J. Chem. Theory Comput.* **1**, 472–483 (2005).
50. M. Lo Conte, K. S. Carroll, The redox biochemistry of protein sulfenylation and sulfinylation. *J. Biol. Chem.* **288**, 26480–26488 (2013).
51. S. H. Kwon, D. R. Pimentel, A. Remondino, D. B. Sawyer, W. S. Colucci, H_2O_2 regulates cardiac myocyte phenotype via concentration-dependent activation of distinct kinase pathways. *J. Mol. Cell. Cardiol.* **35**, 615–621 (2003).
52. F. H. Messerli, S. F. Rimoldi, S. Bangalore, The transition from hypertension to heart failure: Contemporary update. *JACC Heart Fail.* **5**, 543–551 (2017).
53. T. Ma, B. Yang, A. Gillespie, E. J. Carlson, C. J. Epstein, A. S. Verkman, Severely impaired urinary concentrating ability in transgenic mice lacking aquaporin-1 water channels. *J. Biol. Chem.* **273**, 4296–4299 (1998).
54. G. Esposito, A. Rapacciuolo, S. V. Naga Prasad, H. Takaoka, S. A. Thomas, W. J. Koch, H. A. Rockman, Genetic alterations that inhibit in vivo pressure-overload hypertrophy prevent cardiac dysfunction despite increased wall stress. *Circulation* **105**, 85–92 (2002).
55. A. Russo, F. Borrelli, *Bacopa monniera*, a reputed nootropic plant: An overview. *Phytomedicine* **12**, 305–317 (2005).
56. C. Kongkeaw, P. Dilokthornsakul, P. Thanarangsarit, N. Limpeanchob, C. Norman Scholfield, Meta-analysis of randomized controlled trials on cognitive effects of *Bacopa monnieri* extract. *J. Ethnopharmacol.* **151**, 528–535 (2014).
57. D. Mathur, K. Goyal, V. Koul, A. Anand, The molecular links of re-emerging therapy: A review of evidence of brahmi (*Bacopa monniera*). *Front. Pharmacol.* **7**, 44 (2016).
58. E. Migliati, N. Meurice, P. DuBois, J. S. Fang, S. Somasekharan, E. Beckett, G. Flynn, A. J. Yool, Inhibition of aquaporin-1 and aquaporin-4 water permeability by a derivative of the loop diuretic bumetanide acting at an internal pore-occluding binding site. *Mol. Pharmacol.* **76**, 105–112 (2009).
59. A. J. Yool, J. Morelle, Y. Cnops, J.-M. Verbavatz, E. M. Campbell, E. A. Beckett, G. W. Booker, G. Flynn, O. Devuyst, AqF026 is a pharmacologic agonist of the water channel aquaporin-1. *J. Am. Soc. Nephrol.* **24**, 1045–1052 (2013).
60. B. A. Baghbaderani, X. Tian, B. H. Neo, A. Burkall, T. Dimezzo, G. Sierra, X. Zeng, K. Warren, D. P. Kovarcik, T. Fellner, M. S. Rao, GMP-manufactured human induced pluripotent stem cells are available for pre-clinical and clinical applications. *Stem Cell Rep.* **5**, 647–659 (2015).
61. P. L. Soong, M. Tiburcy, W. H. Zimmermann, Cardiac differentiation of human embryonic stem cells and their assembly into engineered heart muscle. *Curr. Protoc. Cell Biol.* **55**, 23.8.1–23.8.21 (2012).
62. E. Krissinel, K. Henrick, Secondary-structure matching (SSM), a new tool for fast protein structure alignment in three dimensions. *Acta Crystallogr. D Biol. Crystallogr.* **60**, 2256–2268 (2014).
63. H. M. Berman, J. Westbrook, Z. Feng, G. Gilliland, T. N. Bhat, H. Weissig, I. N. Shindyalov, P. E. Bourne, The protein data bank. *Nucleic Acids Res.* **28**, 235–242 (2000).
64. A. Waterhouse, M. Bertoni, S. Bienert, G. Studer, G. Tauriello, R. Gumienny, F. T. Heer, T. A. P. de Beer, C. Rempfer, L. Bordoli, R. Lepore, T. Schwede, SWISS-MODEL: Homology modelling of protein structures and complexes. *Nucleic Acids Res.* **46**, W296–W303 (2018).
65. M. Pellegrini-Calace, T. Maiwald, J. M. Thornton, PoreWalker: A novel tool for the identification and characterization of channels in transmembrane proteins from their three-dimensional structure. *PLOS Comput. Biol.* **5**, e1000440 (2009).
66. Y. Dehouck, J. M. Kwasigroch, D. Gilis, M. Rooman, PoPMuSiC 2.1: A web server for the estimation of protein stability changes upon mutation and sequence optimality. *BMC Bioinformatics* **12**, 151 (2011).
67. K. G. Tina, R. Bhadra, N. Srinivasan, PIC: Protein interactions calculator. *Nucleic Acids Res.* **35**, W473–W476 (2007).
68. R. Wintjens, J. Liévin, M. Rooman, E. Buisine, Contribution of cation-π interactions to the stability of protein-DNA complexes. *J. Mol. Biol.* **302**, 395–410 (2000).
69. O. Bergmann, S. Jovinge, Isolation of cardiomyocyte nuclei from post-mortem tissue. *J. Vis. Exp.* **65**, 4205 (2012).
70. O. Bergmann, S. Zdunek, K. Alkass, H. Druid, S. Bernard, J. Frisén, Identification of cardiomyocyte nuclei and assessment of ploidy for the analysis of cell turnover. *Exp. Cell Res.* **317**, 188–194 (2011).
71. C. Kulahoglu, A. Bräutigam, Quantitative transcriptome analysis using RNA-seq. *Methods Mol. Biol.* **1158**, 71–91 (2014).
72. M. I. Love, W. Huber, S. Anders, Moderated estimation of fold change and dispersion for RNA-seq data with DESeq2. *Genome Biol.* **15**, 550 (2014).
73. D. W. Huang, B. T. Sherman, R. A. Lempicki, Bioinformatics enrichment tools: Paths toward the comprehensive functional analysis of large gene lists. *Nucleic Acids Res.* **37**, 1–13 (2009).
74. D. W. Huang, B. T. Sherman, R. A. Lempicki, Systematic and integrative analysis of large gene lists using DAVID bioinformatics resources. *Nat. Protoc.* **4**, 44–57 (2009).
75. X. Jiao, B. T. Sherman, D. W. Huang, R. Stephens, M. W. Baseler, H. C. Lane, R. A. Lempicki, DAVID-WS: A stateful web service to facilitate gene/protein list analysis. *Bioinformatics* **28**, 1805–1806 (2012).
76. J. Vandesompele, K. De Preter, F. Pattyn, B. Poppe, N. Van Roy, A. De Paepe, F. Speleman, Accurate normalization of real-time quantitative RT-PCR data by geometric averaging of multiple internal control genes. *Genome Biol.* **3**, RESEARCH0034.1 (2002).
77. N. Hermida, A. Markl, J. Hamelet, T. Van Assche, A. Vanderper, P. Herijgers, M. van Bilsen, D. Hilfiker-Kleiner, G. Noppe, C. Beauloye, S. Horman, J.-L. Balligand, HMGCoA reductase inhibition reverses myocardial fibrosis and diastolic dysfunction through AMP-activated protein kinase activation in a mouse model of metabolic syndrome. *Cardiovasc. Res.* **99**, 44–54 (2013).
78. F. Aboubakar Nana, D. Hoton, J. Ambroise, M. Lecocq, M. Vanderputten, Y. Sibille, B. Vanaudenaerde, C. Pilette, C. Bouzin, S. Ocak, Increased expression and activation

of FAK in small-cell lung cancer compared to non-small-cell lung cancer. *Cancers* **11**, 1526 (2019).
79. F. J. Alvarez-Leefmans, J. J. Herrera-Pérez, M. S. Marquez, V. M. Blanco, Simultaneous measurement of water volume and pH in single cells using BCECF and fluorescence imaging microscopy. *Biophys. J.* **90**, 608–618 (2006).
80. M. R. Ruggiero, S. Baroni, S. Pezzana, G. Ferrante, S. Geninatti Crich, S. Aime, Evidence for the role of intracellular water lifetime as a tumour biomarker obtained by in vivo field-cycling relaxometry. *Angew. Chem. Int. Ed. Engl.* **57**, 7468–7472 (2018).
81. M. R. Ruggiero, S. Baroni, S. Aime, S. Geninatti Crich, Relaxometric investigations addressing the determination of intracellular water lifetime: A novel tumour biomarker of general applicability. *Mol. Phys.* **117**, 968–974 (2019).
82. M. Balteau, A. Van Steenbergen, A. D. Timmermans, C. Dessy, G. Behets-Wydemans, N. Tajeddine, D. Castanares-Zapatero, P. Gilon, J.-L. Vanoverschelde, S. Horman, L. Hue, L. Bertrand, C. Beauloye, AMPK activation by glucagon-like peptide-1 prevents NADPH oxidase activation induced by hyperglycemia in adult cardiomyocytes. *Am. J. Physiol. Heart Circ. Physiol.* **307**, H1120–H1133 (2014).

Acknowledgments: We thank A. Daumerie and F. Aboubakar for help with the tyramide staining (for the human myocardial tissue immunohistochemistry); H. Chae for helping with the laser-confocal fluorescence microscopy measurements; S. Baroni and M. Russo for helping with the ^{1}H-NMR relaxometric experiments; Y. Cnops and S. Druart for handling of the *Aqp1* mice; J. V. Pei for contributing in silico modeling expertise; and A. Van Steenbergen, J. Dontaine, C. Dufeys, and C. de Meester for help with handling the human myocardial biopsies. Generation of the GMP line LiPSC-GR1.1 was supported by the NIH Common Fund Regenerative Medicine Program. The NIH Common Fund and the National Center for Advancing Translational Sciences (NCATS) are joint stewards of the LiPSC-GR1.1 resource. **Funding:** This work was supported by grant CR J023516F from FRS-FNRS, AGR X100218F, and X500220F from WELBIO, and ARC1621-074 from Federation Wallonie Bruxelles to J.-L.B. S.H. is senior research associate, and L.B., J.-C.J., and P.G. are research directors from FRS-FNRS, Belgium. C. Beauloye was a clinical Master Specialist from FRS-FNRS, Belgium. L.Y.M.M. and C.F. are "Chargé de Recherche" of the FRS-FNRS, Belgium. Work in the H.L.R. laboratory is supported by an Odysseus grant (90663) from Research Foundation Flanders (FWO). Work in the A.Y. laboratory is supported by Australian Research Council grant 19ARC_DP190101745. O.B. is supported by the Center for Regenerative Therapies Dresden, the Karolinska Institutet, the Swedish Research Council, the Ragnar Söderberg Foundation, and the Åke Wiberg Foundation. O.D. is supported by the ARC1621-074 from Federation Wallonie Bruxelles, the Swiss National Centre of Competence in Research Kidney Control of Homeostasis (NCCR Kidney.CH) program, and the Swiss National Science Foundation (310030_189044). W.H.Z. and M.T. are supported by the DFG (German Research Foundation: EXC 2067/1, SFB1002 C04, and S01), the DZHK (German Center for Cardiovascular research), and the Fondation Leducq. Additional funding was provided by the National Institute on Aging of the NIH grant R21 AG06307, Brigham and Women's Hospital Health and Technology Innovation Award, and Brigham Biomedical Research Institute Fund to Sustain Research Excellence. L.B. and J.-L.B. are investigators of the WELBIO Institute. **Author contribution:** J.-L.B. conceived the original hypothesis. J.-L.B. and V.M. conceived the experiments with input from O.D. J.-L.B. supervised the project. J.-L.B. and V.M. planned the experiments and analyzed the results. V.M., H.E., and D.D.M. carried out the core of the experiments. E.L.R. carried out the RNA-seq and RT-qPCR on the hypertrophic human samples and analyzed the output with H.L.R. R.B. performed the structural analysis and interpreted the data with D.G. and M.R. L.Y.M.M. measured specific transcript levels in mouse and human tissues with S.H. B.S. and T.M. developed and provided the HyPer-3 biosensor and experimental protocols. J.-P.D., V.M., and D.D.M performed the HyPer-3 measurements and analyzed them with J.-C.J. R.B. and D.D.M. carried out the osmotic myocyte volume experiments with P.G. D.D.M., V.M., A.G., and S.G.-C. performed the ^{1}H-NMR relaxometry experiments. M.T. carried out the experiments on iPSC and EHM and analyzed them with W.H.Z. P.H.C. carried out the oocytes swelling assays and analyzed them with A.Y. H.E. and C.F. performed echocardiographic measurements with guidance from C. Beauloye. D.D.M., V.M., and C.F. performed immunoblotting and protein synthesis assays with guidance from L.B. D.D.M. and V.M. performed the PLA assays with the help of C. Bouzin. F.D.Z. performed red blood cells measurements with the help of D.B. H.D. expanded and provided the *Aqp1* mice under the supervision of O.D. O.B. provided cadaveric human cardiac tissue and advice on myocyte nuclei isolation. J.-L.V. provided patient cardiac biopsies and clinical echocardiographic data. V.M. and J.-L.B wrote the manuscript. L.Y.M.M. worked on illustration of the data. All authors discussed the results, provided critical feedback, contributed to the writing, or commented on the manuscript. **Competing interests:** The authors declare that they have no competing interests. **Data and materials availability:** All data associated with this study are available in the main text or the Supplementary Materials. All the data of RNA-seq have been registered and submitted to the EMBL-EBI European Nucleotide Archive (ENA) with accession number PRJEB36807.

Submitted 30 May 2019
Resubmitted 24 December 2019
Accepted 31 August 2020
Published 7 October 2020
10.1126/scitranslmed.aay2176

Citation: V. Montiel, R. Bella, L. Y. M. Michel, H. Esfahani, D. De Mulder, E. L. Robinson, J.-P. Deglasse, M. Tiburcy, P. H. Chow, J.-C. Jonas, P. Gilon, B. Steinhorn, T. Michel, C. Beauloye, L. Bertrand, C. Farah, F. Dei Zotti, H. Debaix, C. Bouzin, D. Brusa, S. Horman, J.-L. Vanoverschelde, O. Bergmann, D. Gilis, M. Rooman, A. Ghigo, S. Geninatti-Crich, A. Yool, W. H. Zimmermann, H. L. Roderick, O. Devuyst, J.-L. Balligand, Inhibition of aquaporin-1 prevents myocardial remodeling by blocking the transmembrane transport of hydrogen peroxide. *Sci. Transl. Med.* **12**, eaay2176 (2020).

Science Translational Medicine

Inhibition of aquaporin-1 prevents myocardial remodeling by blocking the transmembrane transport of hydrogen peroxide

Virginie Montiel, Ramona Bella, Lauriane Y. M. Michel, Hrag Esfahani, Delphine De Mulder, Emma L. Robinson, Jean-Philippe Deglasse, Malte Tiburcy, Pak Hin Chow, Jean-Christophe Jonas, Patrick Gilon, Benjamin Steinhorn, Thomas Michel, Christophe Beauloye, Luc Bertrand, Charlotte Farah, Flavia Dei Zotti, Huguette Debaix, Caroline Bouzin, Davide Brusa, Sandrine Horman, Jean-Louis Vanoverschelde, Olaf Bergmann, Dimitri Gilis, Marianne Rooman, Alessandra Ghigo, Simonetta Geninatti-Crich, Andrea Yool, Wolfram H. Zimmermann, H. Llewelyn Roderick, Olivier Devuyst and Jean-Luc Balligand

Sci Transl Med **12**, eaay2176.
DOI: 10.1126/scitranslmed.aay2176

Help for hypertrophy

One way that cardiomyocytes respond to injury or stress is by increasing in size (hypertrophy). Montiel *et al.* studied the role of oxidative stress in myocardial hypertrophy. They saw that the water channel aquaporin-1 (AQP1) was increased in mouse and human hypertrophic heart tissue and that AQP1 regulated hydrogen peroxide transport within myocytes. Deletion or pharmacological blockade of AQP1 abrogated hypertrophy in response to d ifferent stressors in cells and in a mouse model of angiotensin II–induced cardiac hypertrophy, identifying a potential therapeutic target for hypertrophic cardiomyopathy.